ALMA MATER STUDIORUM
UNIVERSITÀ DI BOLOGNA

DEPARTMENT OF ELECTRICAL, ELECTRONIC, AND INFORMATION ENGINEERING "GUGLIELMO MARCONI" - DEI

SECOND CYCLE DEGREE
AUTOMATION ENGINEERING

MODELING AND CONTROL FOR THE ITER GAS INJECTION SYSTEM

Dissertation in Modeling and Simulation of Mechatronic Systems

Supervisor

Prof. Alessandro Macchelli

Defended by

Dante Piotto

Co-Supervisors

Anna Trang Vu

Luca Zabeo

V Graduation Session / March / 2025

Academic Year 2023/2024

Contents

Abstract **7**

1 Introduction **9**
1.1 The ITER Project . . . 11
1.2 The ITER Gas Injection System . . . 12

2 Port-Hamiltonian Systems **15**
2.1 Modelling: finite dimensional case . . . 15
2.1.1 Interconnection structure . . . 16
2.1.2 Energy storage . . . 18
2.1.3 Dissipation . . . 18
2.1.4 Port-Hamiltonian dynamics . . . 18
2.2 Control: finite dimensional case . . . 20
2.2.1 Interconnection and Damping Assignment . . . 20
2.2.2 Solving the matching equation . . . 21
2.3 Modelling: inifinite dimensional case . . . 22
2.3.1 Energy storage . . . 23
2.3.2 Dissipation . . . 24

3 MFC Valve model **27**
3.1 Plunger model . . . 27
3.1.1 Mechanical subsystem . . . 28
3.1.2 Electrical subsystem . . . 28
3.1.3 Coupling the subsystems . . . 28
3.2 Flow characteristic . . . 29
3.2.1 Discharge coefficient . . . 30
3.2.2 Flow coefficient . . . 30
3.3 Sensor model . . . 31
3.4 Comparison of the simulation model with experimental data . . . 33

4 Pipe model **35**
4.1 Model description . . . 35
4.2 PH formulation of the pipe model . . . 36
4.3 Coupling witht valve model . . . 36
4.4 Comparison with experimental data . . . 37
4.5 Alternative pipe models . . . 38
4.5.1 Advection-Diffusion model . . . 39
4.5.2 Euler model . . . 39

5 MFC Valve control **41**
5.1 Observer 41
5.2 Reference Generation 41
5.3 IDA-PBC controller 43
5.4 Alternative control functions 44
5.4.1 Parametrized IDA 45
5.4.2 Non-Parametrized IDA 46

6 Conclusion **49**

Appendix **49**

A Solution of transport PDEs **51**

List of Figures

1.1 Global average temperature change, By RCraig09 - Own work, CC BY-SA 4.0, wikimedia commons . . . 9
1.2 Schematic of the working of a Tokamak, [21] . . . 10
1.3 Schematic of the working of a Stellarator, [3] . . . 11
1.4 Schematic of the magnetic field in a magnetic mirror device, By User:WikiHelper2134, CC BY-SA 3.0, wikimedia commons . . . 11
1.5 injection points of the GIS in the vacuum vessel, [11] . . . 12
1.6 schematic of a gas valve box . . . 12

2.1 Analogous representation of mechanical and physical systems . . . 15
2.2 general bond graph of a PH system . . . 16
2.3 Magnetically levitated ball . . . 19

3.1 Side section of an MFC valve . . . 27
3.2 Bond graph of the electromechanical dynamics of the solenoid actuated valve 29
3.3 Inductance function $L(q)$ . . . 30
3.4 Voltage-flow relations at steady state from SWIP data . . . 30
3.5 simulation model voltage-flow relation at steady state . . . 31
3.6 Schematic of the MFC valve flow meter . . . 31
3.7 Comparison of flow sensor data with pressure downstream of MFC valve . 32
3.8 Simulink scheme of the MFC valve model. . . . 33
3.9 Comparison of simulated high flow valve with experimental data, H_2 . . . 34
3.10 Comparison of simulated high flow valve with experimental data, Ar . . . 34

4.1 bond graph of the coupled pipe and valve . . . 36
4.2 Pressure at the pipe inlet . . . 37
4.3 Pressure at the end of the pipe . . . 38
4.4 Pressure in the vacuum vessel . . . 38

5.1 observer estimates of valve state . . . 42
5.2 observer estimates of valve state . . . 42
5.3 result of IDA-PBC control on high flow valve with H_2 . . . 44
5.4 result of IDA-PBC control on high flow valve with Ar . . . 44
5.5 high flow valve with step force disturbance at $t = 3s$, H_2 . . . 44
5.6 low flow valve with step force disturbance at $t = 3s$, Ar . . . 45
5.7 Controller Simulink model . . . 45
5.8 Observer Simulink model . . . 45

Abstract

This thesis presents the modelling and control of the ITER Gas Injection System. The non-linear models for both the valve and the pipe are formulated using the port-Hamiltonian approach. The primary focus of this study is the valve model, which incorporates both the mechanical and electrical domains, as well as the nonlinear coupling between them. An observer is designed for the valve to reconstruct the system states from the gas flow measurement at the valve output. A passivity-based controller is then developed to regulate gas flow into the tokamak vacuum vessel. The valve model is implemented in the ITER simulation platform PCSSP and validated with experimental data. The control algorithm is implemented and tested in simulation.

Chapter 1

Introduction

Talk about fusion energy, history of Tokamaks, ITER project.

The world is undeniably undergoing a climate crisis that requires urgent action [1]. The energy sector is one of the main contributors to the greenhouse gas emissions that are causing this crisis, and it is therefore crucial to transition to cleaner energy sources [20]. Moreover, we heavily rely on fossil fuels, which are limited in their quantity and may in a not so distant future run out [4]. Research in fusion energy aims to solve these

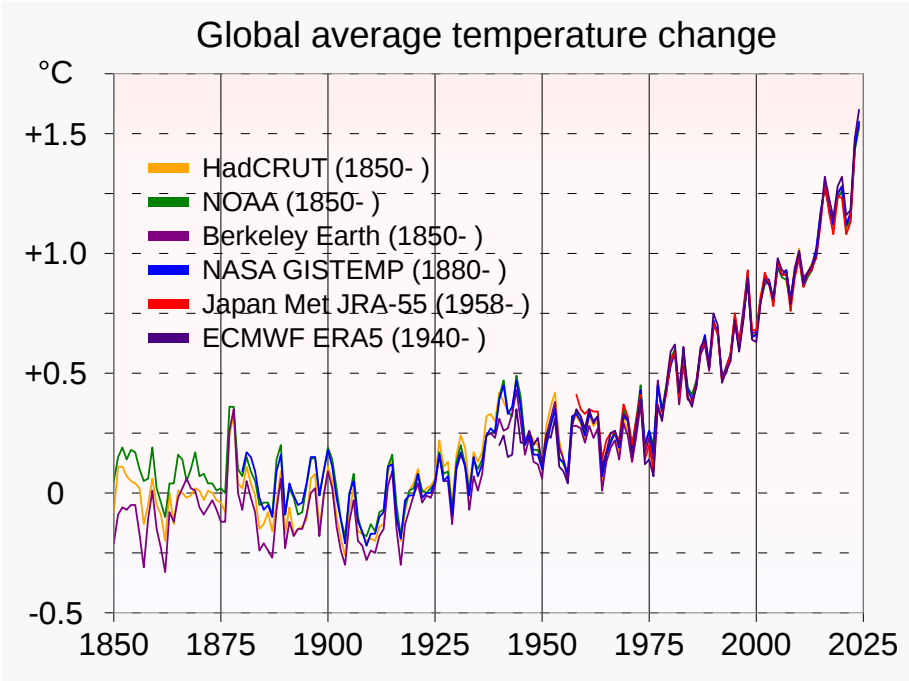

Figure 1.1: Global average temperature change, By RCraig09 - Own work, CC BY-SA 4.0, wikimedia commons

problems. Nuclear fusion is the process that powers the stars, and it is a very promising source of energy for the future of humanity. Interest in the potential of nuclear fusion for the production of energy started in the Los Alamos Laboratory, during the Manhattan project [5]. Nuclear fusion is a nuclear reaction, in which the nuclei of two or more atoms combine to form a larger nucleus and other nuclei/neutrons as byproducts. The difference in mass between the original atoms and the combined product is manifested as excess energy, stemming from the difference in nuclear binding energy before and after

the reaction. To achieve nuclear fusion, atoms require enough energy to overcome the natural barrier stopping them from combining on their own [12]. This requires conditions of extreme pressure and temperature. These conditions are achieved in star cores, nuclear weapons, and fusion power devices. In order to harness the power of fusion energy, the highly exothermic fusion reactions must be contained. There are two main methods that are used to achieve confinement of plasma:

- Inertial confiemeent, where the plasma is compressed to extremely high densities, and the inertia of the plasma particles is enough to confine them to within the reactor vessel. This implies that the fusion reactions would happen in a pulsed fashion, for extremely short durations (around 100 ps) [14].
- Magnetic confinement, where the plasma is confined by magnetic fields which act upon the charged particles in the plasma. Different tipes of devices have been ideated and tested using magnetic confinement:
  - Tokamaks: toroidal device, using a combination of magnets to confine the plasma within a toroidal shape. This has been the most popular approach so far

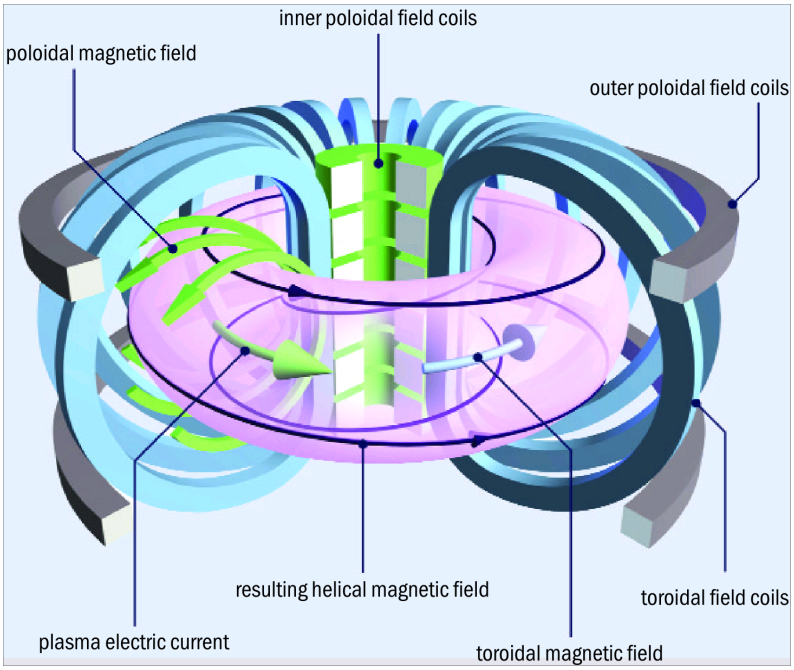

Figure 1.2: Schematic of the working of a Tokamak, [21]

  - Stellarators: similar to tokamas, they use a carefully designed set of magnets to address some of the instability challenges faced by tokamaks by creating a twisted magnetic field configuration. The challenge is shifted from control of instabilities to geometric design and fabrication of the machine
  - Mirror devices present a cylindrical geometry, with magnets designed to suppress longitudinal leakage of plasma through magnetic forces parallel to the axis of the cilinder. The main advantage of such devices is the ease of construction as compared to tokamaks and stellarators [15]

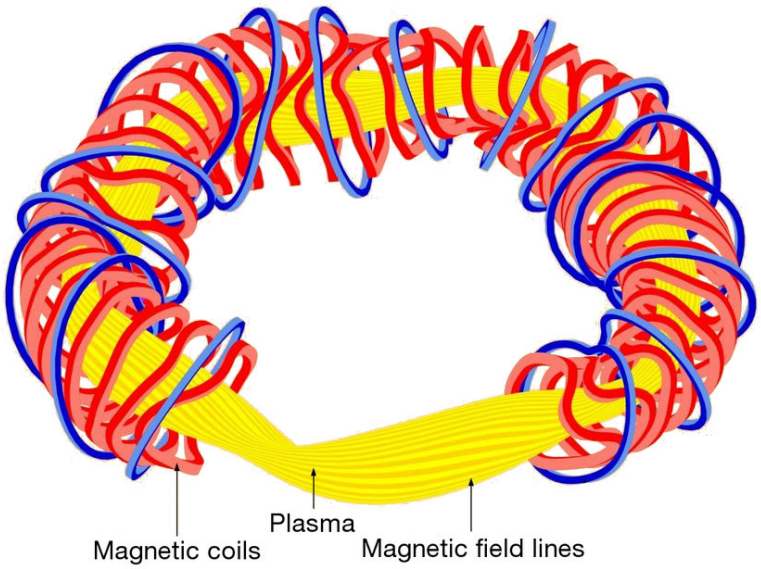

Figure 1.3: Schematic of the working of a Stellarator, [3]

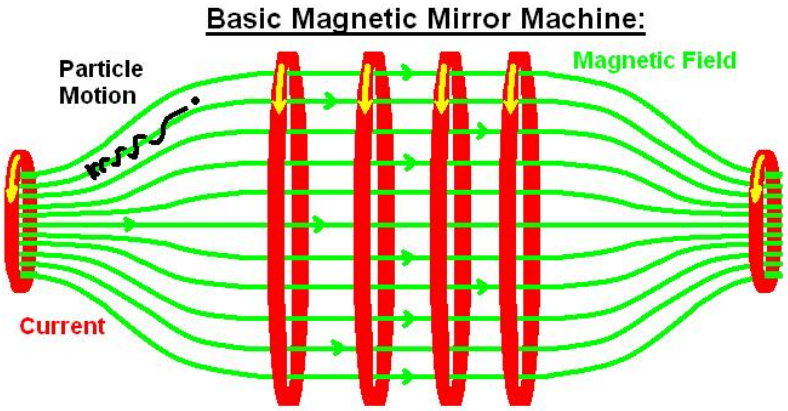

Figure 1.4: Schematic of the magnetic field in a magnetic mirror device, By User:WikiHelper2134, CC BY-SA 3.0, wikimedia commons

The main challenge in fusion remains to this day to achieve a net energy gain from the fusion reactions.

1.1 The ITER Project

The work presented in this thesis was developed during an internship at ITER. ITER is an international research project based in Cadarache, in the south of France. Over the course of decades, the ITER Members – China, the European Union, India, Japan, Korea, Russia and the United States – have collaborated with the main goal of building a tokamak capable of achieving a ten-fold return on power. This is to be achieved through a "burning plasma": the heat produced by the fusion reaction should be sufficiently contained within the plasma itself to continouslly fuelk it and provide the main source of heating to achieve prolonged fusion. Other goals of the project are to contribute to the demonstration and development of technologies for fusion power plants, test tritium

breeding (producing tritium within the vacuum vessel exploiting the fusion reaction), and demonstrate the safety of nuclear fusion devices.

The ITER project is currently in the assembly phase, with the first plasma expected to be achieved in 2034. The project is divided into several systems, each responsible for a different aspect of the operation of the tokamak. The systems are designed to work together to achieve the main goals of the project. This work focuses on the Gas Injection system.

1.2 The ITER Gas Injection System

The ITER Gas Injection System (GIS) is the system responsible for supplying gas to the vacuum vessel, for both fuelling purposes and for impurity injection. It will play a key role in the plasma density control performed by the Plasma Control System (PCS) [6]. This work focuses on the modelling and control of the ITER GIS, with particular attention to the valves that supply gas to the vacuum vessel. The main challenge in control of the GIS is given by the delay introduced into the system by the length of the pipes connecting the fuelling valves to the vacuum vessel. This warrants the development of accurate models and suitable control algorithms for the system. A testbench was built at South Western Institute of Physics to characterize the response of the GIS, and the data was used to validate the valve model proposed in this thesis. The GIS is composed of 10 Gas Valve Boxes (GVB), each consisting of 6 Mass Flow Controlled (MFC) valves, and the pipe system connecting the GVBs to the vacuum vessel (VV). This work proposes

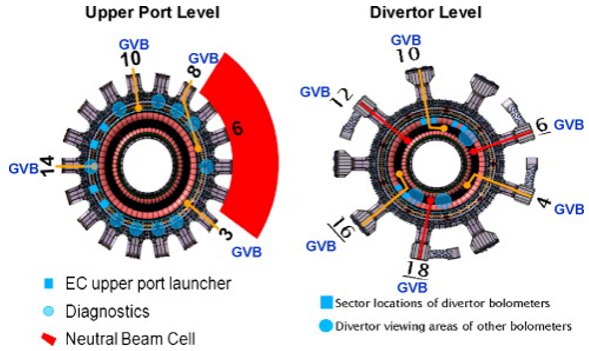

Figure 1.5: injection points of the GIS in the vacuum vessel, [11]

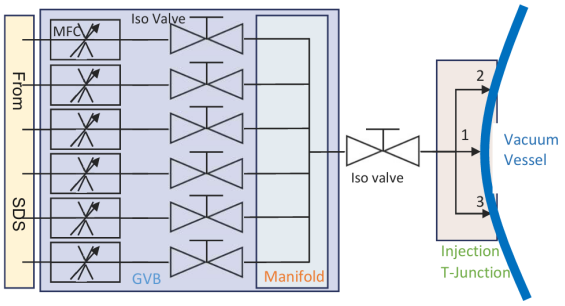

Figure 1.6: schematic of a gas valve box

accurate models and an advanced control algorithm to guarantee the performance of the GIS. The port-Hamiltonian approach [13, 28], with its modular feature and stability analysis advantages, is an appropriate method for modelling of multiphysic systems, such as the GIS. Different from the levitated ball system in [28],Sec.2.6, non-linear coupling is considered between the mechanical and electrical domains in this application.

The control strategy Interconnection and Damping Assignment - Passivity Based Control (IDA-PBC) proposed in this paper was initially presented in [17]. Control of a similarly class of the considered systems has been discussed in [29, 23]. The solutions in the aforementioned rely on the linear structure of the considered systems, which is not present in the case discussed in this paper. In [24] it is shown that integral control can be combined with the IDA-PBC technique to improve robustness of the control. The IDA-PBC control algorithm developed in this work requires a full knowledge of the system states,

therefore, an observer is also designed for the valve to reconstruct the these states from the gas flow measurement at the valve output.

The proposed valve model is implemented in the ITER simulation platform PCSSP [22] and validated with experimental data from the testbench at the South Western Institute of Physics (SWIP). The control algorithm is implemented and tested in simulation. The rest of this work is organized as follows:

- Chapter 2 presents the theoretical framework for port-controlled Hamiltonian systems, which is used throughout the rest of the thesis
- Chapter 3 presents the dynamic model developed for the MFC valves and compares it to the experimental data from SWIP.
- Chapter 4 discusses the pipe model developed at CEA and compares it with the experimental data from SWIP, and proposes some alternative models that could be employed in its place.
- Chapter 5 presents the control scheme developed for the MFC valve and showcases its performance and robustness for step references.

Chapter 2

Port-Hamiltonian Systems

Port-Hamiltonian system theory [29] is born of the combination of the Bond Graph approach to modelling [19],[10] with the geometric Hamiltonian formulation of mechanics [2]. The core idea is to model systems as an interconnection of different basic elements, the interaction of which is determined by an *interconnection structure*.

This approach to modelling and control is quite general, well suited to multi-physics systems, scalable and versatile. It provides great insight into the behaviour of dynamcal systems and among its advantages makes one of the main problems in system theory –stability analysis– quite intuitive. In this chapter we deal with the simpler cases of finite dimensional systems defined on $\mathbb{R}^n$ and infinite dimensional systems treated through differential operators, however there exist frameworks based on differential geometry where finite dimensional systems are treated in the case of state spaces defined on manifolds and infinite dimensional systems are approached through the use of differential forms. These approaches are more general, however they introduce a rather heavy formalism that is outside the scope of this work.

In the following, concepts in port-Hamiltonian modelling and control will be displayed, starting from bond graph modelling.

2.1 Modelling: finite dimensional case

We start by considering two classical systems: the mass-spring-damper and the RLC circuit in Figure 2.1. As is already known from bond graph modelling, the representation

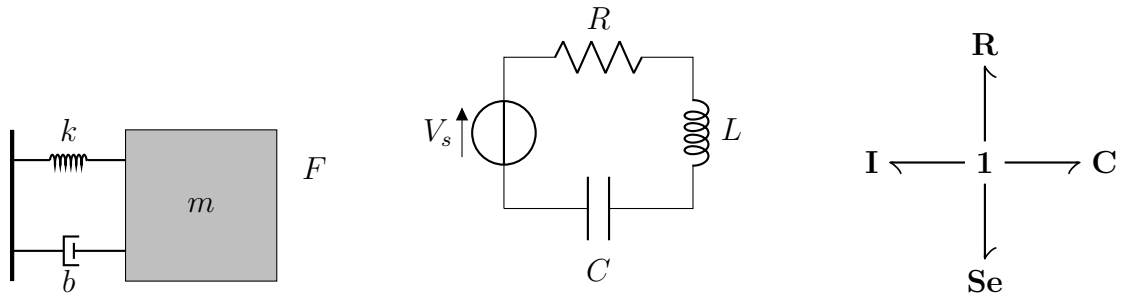

(a) mass-spring-damper (b) RLC circuit (c) bond graph for both systems

Figure 2.1: Analogous representation of mechanical and physical systems

for both systems is analogous: they both present inertial, capacitive, and dissipative elements, all sharing the same flow (velocity in the mechanical case, electric current in the electric case). In the port-Hamiltonian philosphy, we would rather see the systems as composed of energy storage (including both capacitive and inertial components), dissipative components, and potentially an external interaction port, interconnected by some structure. The bond graph in Figure 2.2 portrays this concept: $\mathcal{S}$ reprents the storage

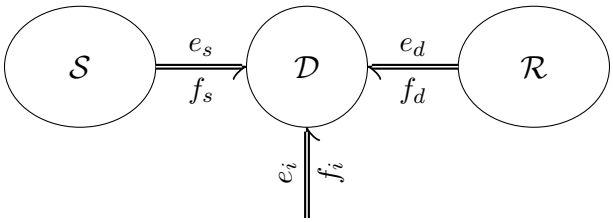

Figure 2.2: general bond graph of a PH system

element, $\mathcal{R}$ the dissipation element and $\mathcal{D}$ the interconnection structure. The concepts of flow and effort are inherited from bond graph theory and are thus typically associated to variables the product of which is instantaneous power. In table 2.1 a classification of flows and efforts in different domains is displayed. In general, we consider an abstract finite(for now)-dimensional vector space of *flows* $\mathcal{F}$, the elements of which we denote as $f \in \mathcal{F}$ and call *flow vectors*. We call the *dual* to this vector space the space of *efforts* $\mathcal{E} = \mathcal{F}^*$ and denote its elements by $e \in \mathcal{E}$. We call the cartesian product of the flow and effort spaces the space of *port variables*. Power is given by the canonical pairing on the space of port variables:

$$P = \langle e|f\rangle \qquad (f, e) \in \mathcal{F} \times \mathcal{E} \tag{2.1}$$

physical domain	flow	effort	storage state
electric	current	voltage	charge
magnetic	voltage	current	flux linkage
potential translation	velocity	force	displacement
kinetic translation	force	velocity	momentum
potential rotation	angular velocity	torque	angular displacement
kinetic rotation	torque	angular velocity	angular momentum
potential hydraulic	volume flow rate	pressure	volume
kinetic hydraulic	pressure	volume flow rate	flow tube momentum

Table 2.1: Domain of classification in port-Hamiltonian framework

2.1.1 Interconnection structure

Definition 2.1 ([8, 29])
A *Dirac structure* on $\mathcal{F} \times \mathcal{E}$ is a subspace $\mathcal{D} \subset \mathcal{F} \times \mathcal{E}$ such that:

1. $\langle e|f\rangle = 0$ for all $(f, e) \in \mathcal{D}$
2. $\dim \mathcal{D} = \dim \mathcal{F}$

Property 1 corresponds to power-conservation: it indicates that the total power flowing through a Dirac structure is zero, i.e. all the Dirac structure does is route power within the system. It can be shown that the maximal dimension the Dirac structure $\mathcal{D}$ can assume maintaining property 1 is $\dim \mathcal{F}$, and thus property 2 says that a Dirac structure is the maximal subspace of $\mathcal{F} \times \mathcal{E}$ ensuring property 1. There is an equivalent definition of Dirac structures which is useful as it generalizes also to infinite-dimensional structure. In order to give this definition, we introduce the *bilinear form* canonically defined on the bond space $\mathcal{F} \times \mathcal{E}$:

$$\ll (f^a, e^a), (f^b, e^b) \gg := \langle e^a | f^b \rangle + \langle e^b | f^a \rangle \tag{2.2}$$

we can now give the following alternative definition of a Dirac structure [8]:

Proposition 2.1
A (constant) Dirac structure on $\mathcal{F} \times \mathcal{E}$ is a subspace $\mathcal{D} \subset \mathcal{F} \times \mathcal{E}$ such that:

$$\mathcal{D} = \mathcal{D}^{\perp} \tag{2.3}$$

where $\mathcal{D}^{\perp}$ is the orthogonal complement of $\mathcal{D}$ with respect to the bilinear form $\ll \cdot, \cdot \gg$:

$$\mathcal{D}^{\perp} = \{(f, e) \in \mathcal{F} \times \mathcal{E} | \ll (f, e), (f\prime, e\prime) \gg = 0 \forall (f\prime, e\prime) \in \mathcal{D}\} \tag{2.4}$$

proof of this proposition can be found in [8].

This additional definition, while it may seem rather abstract, has the benefit of not being tied to finite-dimensional vetor spaces, thus allowing for definition of Dirac strucutres for infinite-dimensional systems. This will be further discussed in section 2.3 of this chapter. Furthermore, the only requirement imposed on flow and effort spaces is that they be vector spaces; for example, in the finite-dimensional case we need not limit ourselves to $\mathbb{R}^n$, but can rather consider for example in rigid body mechanics, the lie algebra of the special euclidean group of $\mathbb{R}^3$ $\mathfrak{se}(3)$ (along with its dual) to represent twists and wrenches.

An very relevant example of Dirac structure is the following:

Proposition 2.2
Let $J : \mathcal{E} \to \mathcal{F}$ be a skew-symmetric linear mapping, that is $J = -J^*$, where $J^* : \mathcal{E} \to \mathcal{F}$ is the adjoint mapping. Then

$$\operatorname{graph} J := \{(f, e) \in \mathcal{F} \times \mathcal{E} | f = Je\} \tag{2.5}$$

is a Dirac structure

Proof. We use the first definition of Dirac structure and verify the two properties. First, we have that for all $(f, e) \in \operatorname{graph} J$:

$$\langle e | f \rangle = \langle e | Je \rangle = \langle J^* e | e \rangle = -\langle e | Je \rangle = 0$$

where the first equivalence is given by the definition of the Dirac structure we are considering, the second by the definition of the adjoint operator of J and the third by the condition that J be skew-symmetric. Property 2 is trivially satisfied as $\dim \operatorname{graph} J = \dim \mathcal{E} = \dim \mathcal{F}$. □

2.1.2 Energy storage

An energy storage is characterized by two elements:

- A physical state $x \in \mathcal{M}$
- An Hamiltonian function $H : \mathcal{M} \to \mathbb{R}$ denoting energy

In the general setting the state space $\mathcal{M}$ is a smooth manifold, however we limit ourselves to consider state-spaces defined on $\mathbb{R}^n$. The vector of flow variables of the energy storing element is given by the time derivative of the state, while the effort is given by the gradient of the Hamiltonian:

$$f_s = -\dot{x} \qquad e_s = \nabla H(x) \tag{2.6}$$

We obtain the following power balance for energy storing elements:

$$\frac{d}{dt}H = -\langle e_s | f_s \rangle = \langle \nabla H(x) | \dot{x} \rangle \tag{2.7}$$

Note that the gradient of the Hamiltonian is a covector and the time derivative of the state is a vector, thus the pairing is well defined.

Remark. the $-$ sign in equation (2.6) is necessary to ensure a consistent power flow convention: $\langle \nabla H | \dot{x} \rangle$ is the power flowing into the storage element, while $\langle e_s | f_s \rangle$ is the power flowing into the Dirac structure.

2.1.3 Dissipation

The dissipation port is characterized by a resistive relation $\mathcal{R}$. This relation is in general in the form

$$R(f_d, e_d) = 0 \tag{2.8}$$

with the property for all (f_d, e_d) satisfying (2.8)

$$\langle e_d | f_d \rangle \leq 0 \tag{2.9}$$

i.e., power only flows into the disspiation element.

Taking into account also the external interaction port, we can write the power balance for the whole system as:

$$\langle e_s | f_s \rangle + \langle e_d | f_d \rangle + \langle e_i | f_i \rangle = 0 \tag{2.10}$$

An updated version of equation (2.7) follows as:

$$\frac{d}{dt}H = \langle e_d | f_d \rangle + \langle e_i | f_i \rangle \tag{2.11}$$

2.1.4 Port-Hamiltonian dynamics

Formally, a port-Hamiltonia system is defined as follows:

Definition 2.2
Consider a state space $\mathcal{X}$ and a port-Hamiltonian

$$H : \mathcal{X} \to \mathbb{R}$$

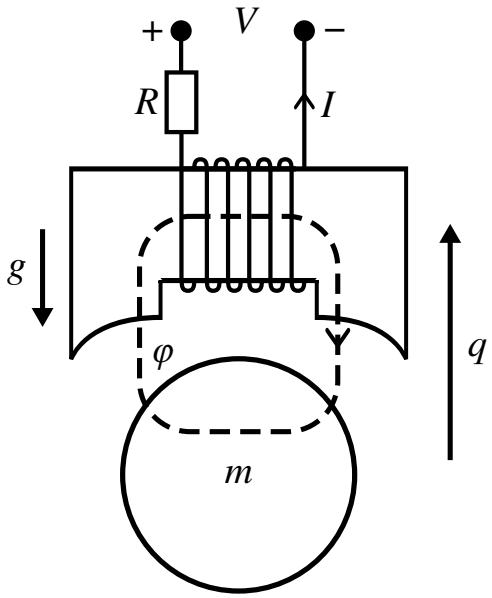

Figure 2.3: Magnetically levitated ball

defining energy-storage. A port-Hamiltonian system on $\mathcal{X}$ is defined by a Dirac structure

$$\mathcal{D} \subset T_x\mathcal{X} \times T_x^*\mathcal{X} \times \mathcal{F}_d \times \mathcal{E}_d \times \mathcal{F}_i \times \mathcal{E}_i$$

having energy storing port $(f_s, e_s) \in T_x\mathcal{X} \times T_x^*\mathcal{X}$ where $T_x\mathcal{X}$ is the tangent space to $\mathcal{X}$ at x and $T_x^*\mathcal{X}$ is the cotangent space(in the case $\mathcal{X} = \mathbb{R}^n$ the tangent space is the space itself), and a resistive structure

$$\mathcal{R} \subset \mathcal{F}_d \times \mathcal{E}_d$$

corresponding to an energy-dissipating port. Its dynamics is specified by:

$$\begin{gathered}(-\dot{x}(t), \nabla H(x(t)), f_d(t), e_d(t), f_i(t), e_i(t)) \in \mathcal{D}(x(t)) \\ (f_d(t), e_d(t)) \in \mathcal{R}(x(t)), \quad t \in \mathbb{R}\end{gathered} \tag{2.12}$$

One useful form in which the system dynamics can present in the case of finite-dimensional systems with state in $\mathbb{R}^n$ is the following:

$$\begin{aligned}\dot{x} &= [J(x) - R(x)]\nabla H(x) + g(x)u \\ y &= g^T(x)\nabla H(x)\end{aligned} \tag{2.13}$$

where $J : \mathbb{R}^n \to \mathbb{R}^{n\times n}$ is a skew-symmetric matrix representing the interconnection of the system, $R : \mathbb{R}^n \to \mathbb{R}^{n\times n}$ is a symmetric, positive semidifinite matrix representing the resistive relation, $u \in \mathbb{R}^m$ is an input to the system and $g(x) : \mathbb{R}^m \to \mathbb{R}^n$ is the input map.

Example 2.1 (Magnetically levitated ball)
Consider the dynamics of an iron ball affected by the magnetic field created by an actuated inductor, shown in Fig. 2.3. The state of the system is given by the height of the ball q, its momentum p, and the flux linkage of the inductor φ. The system Hamiltonian is given by:

$$H(q, p, \varphi) = mgq + \frac{p^2}{2m} + \frac{\varphi^2}{2L(q)}$$

The dynamics of the system is given by:

$$\begin{bmatrix} \dot{q} \\ \dot{p} \\ \dot{\varphi} \end{bmatrix} = \begin{bmatrix} 0 & 1 & 0 \\ -1 & 0 & 0 \\ 0 & 0 & -R \end{bmatrix} \begin{bmatrix} \frac{\partial H}{\partial q} \\ \frac{\partial H}{\partial p} \\ \frac{\partial H}{\partial \varphi} \end{bmatrix} + \begin{bmatrix} 0 \\ 0 \\ 1 \end{bmatrix} V \tag{2.14}$$

We may note that the coupling between the mechanical and magnetic domains happens through the Hamiltonian.

2.2 Control: finite dimensional case

2.2.1 Interconnection and Damping Assignment

IDA-PBC control was introduced in [18] as a method to synthesize stabilizing controllers for port-controlled Hamiltonian systems in input output-form as in equation (2.13). The control design objective of interconnection and damping assignment passivity-based control is to obtain a closed loop PH system of the form

$$\dot{x} = [J_d(x) - R_d(x)]\nabla H_d(x) \tag{2.15}$$

where J_d, R_d and H_d are desired interconnection and damping matrices and Hamiltonian function of the closed loop system respectively. The main proposition of IDA-PBC is the following [18, 8]:

Proposition 2.3
Consider the system (2.13), assume there are matrices $g^{\perp}(x)$, $J_d(x) = -J_d^T(x)$, $R_d(x) = R_d^T(x)$ and a function $H_d(x)$ that verify the following PDE:

$$g^{\perp}(x)[J(x) - R(x)]\frac{\partial H}{\partial x} = g^{\perp}(x)[J_d(x) - R_d(x)]\frac{\partial H_d}{\partial x} \tag{2.16}$$

where $g^{\perp}(x)$ is a full rank left annihilator of $g(x)$, i.e. $g^{\perp}(x)g(x) = 0$, and $H_d(x)$ is such that

$$x^{\star} = \arg\min H_d(x) \tag{2.17}$$

with $x^{\star}$ the desred equilibrium to be stabilized. Then, the closed-loop system (2.13) with $u = \beta(x)$, where

$$\beta(x) = [g^T(x)g(x)]^{-1}g^T(x)\left\{[J_d(x) - R_d(x)]\frac{\partial H_d}{\partial x} - [J(x) - R(x)]\frac{\partial H}{\partial x}\right\}$$

takes the port-Hamiltonian form (2.15), with $x^{\star}$ a (locally) stable equilibrium. It will be *asymptotically* stable if, in addition, $x^{\star}$ is an isolated minimum of $H_d(x)$ and the largest invariant set under the closed-loop dynamics (2.15) contained in

$$\left\{x \in \mathcal{X} \,\middle|\, \frac{\partial^T H_d}{\partial x} R_d(x) \frac{\partial H_d}{\partial x} = 0\right\}$$

equals $\{x^{\star}\}$.

We may view IDA-PBC as adding an energy function $H_a(x)$ to the system through the control port, thus obtaining at closed loop $H_d(x) = H(x) + H_a(x)$. On top of adding a term to the energy we also may formulate the modification to the damping and injection matrices in terms of addition of other interconnection and damping matrices, namely $J_d(x) = J(x) + J_a(x)$ and $R_d(x) = R(x) + R_a(x)$. Equation (2.16) can therefore be rewritten as:

$$[R_a - J_a]\frac{\partial H}{\partial x} + gu(x) = [J + J_a - R - R_a]\frac{\partial H_a}{\partial x} \tag{2.18}$$

2.2.2 Solving the matching equation

Equation (2.16) is called the *matching equation* as it corresponds to imposing that the closed-loop dynamics match the desired dynamics. The key step in IDA-PBC control synthesis is solving this PDE. There are three main ways to go about solving this equation:

1. *Algebraic IDA*: The simplest method is to fix a desired energy function, satisfying the conditions of proposition 2.3, and solve the matching equation for the desired interconnection and damping matrices. This turns the problem into a set of algebraicn equations in $J_d(x)$ and $R_d(x)$ which if solvable are quite easy to solve.

2. *Parametrized IDA*: This approach consists in restricting the closed loop energy function to a certain class, without however fixing it completely. This results in a simpler PDE with some constraints on $J_d(x)$ and $R_d(x)$.

3. *Non-Parametrized IDA*: The most cumbersome of the three from a computational point of view, this approach consists in fixing the desired interconnection and damping matrices $J_d(x)$ and $R_d(x)$, – as well as $g^{\perp}(x)$ – (hence the name Interconnection and Damping Assignment), yielding a PDE whose solution is a family of admissible closed-loop energy functions. Among these, one must be chosen that satisfies the conditions of proposition 2.3

Example 2.2 (control of a magnetically levitated ball)
Consider the magnetically levitated ball of Example 2.1. We set as our control design goal to stabilize the ball at some height $q^{\star}$. We employ the IDA-PBC approach, in particular we may elect to use the *Non-Parametrized IDA* as is done for this system in [29]. It can be observed that an obstacle in the control of the system is that the interconnection matrix J does not couple the mechanical portion of the system with the electromagnetic dynamics, through which the system is controlled. For this reason, we pick as our desired interconnection matrix

$$J_d = \begin{bmatrix} 0 & 1 & 0 \\ -1 & 0 & -\alpha \\ 0 & \alpha & 0 \end{bmatrix} \tag{2.19}$$

By plugging this into the *matching equation* (2.18) (considering $R_d = 0$) we get the following PDE system:

$$\begin{aligned} \frac{\partial H_a}{\partial p} &= 0 \\ -\frac{\partial H_a}{\partial q} - \alpha\frac{\partial H_a}{\partial \varphi} &= \alpha\frac{(1-q)}{k}\varphi \\ \alpha\frac{\partial H_a}{\partial p} - R\frac{\partial H_a}{\partial \varphi} &= \alpha\frac{p}{m} + u(x) \end{aligned} \tag{2.20}$$

The third equation prescribes the control law, whereas the second can be resolved to obtain:

$$H_a(q,\varphi) = -\frac{\varphi^3}{6k\alpha} - \frac{1}{2k}(1-q)\varphi^2 + \Phi(q+\frac{\varphi}{\alpha}) \tag{2.21}$$

with $\Phi(\cdot)$ to be chosen such that condition (2.17) is satisfied.

2.3 Modelling: inifinite dimensional case

As was anticipated in section 2.1, the port-Hamiltonian framework has been extended to include infinite-dimensional systems as well. In this section a framework for distrubuted parameter systems on 1D domains is presented, following the tractation in [8].

The definitions in section 2.1 were kept as general as possible to allow for use in the finite-dimensional case as well as in the infinite-dimensional case. We therefore need only specify some details to show how they adapt to the infinite-dimensional case. Firstly, we consider as the spatial domain the set $Z = [a,b]$ with $a,b \in \mathbb{R}$, with boundary $\partial Z = \{a,b\}$. The spaces within which flows and efforts lie require care in their definition to be able to obtain Dirac structures. We start by considering flows and efforts in the spatial domain as smooth functions from the domain Z to $\mathbb{R}^n$:

$$f_Z(z) \in C^\infty(Z;\mathbb{R}^n) \qquad e_Z(z) \in C^\infty(Z;(\mathbb{R}^n)^*) \tag{2.22}$$

We define two *boundary port variables* as the restriction of flows and efforts to the boundary of the domain:

$$f_\partial = \begin{bmatrix} f_Z(a) \\ f_Z(b) \end{bmatrix}, \quad e_\partial = \begin{bmatrix} e_Z(a) \\ e_Z(b) \end{bmatrix} \tag{2.23}$$

We define the *space of flows* as:

$$\mathcal{F} = \left\{ f = \begin{bmatrix} f_Z \\ f_\partial \end{bmatrix} \in C^\infty(Z;\mathbb{R}^n) \times \mathbb{R}^{a,b} \right\} \tag{2.24}$$

and accordingly the *space of efforts* as its dual:

$$\mathcal{E} = \left\{ e = \begin{bmatrix} e_Z \\ e_\partial \end{bmatrix} \in C^\infty(Z;(\mathbb{R}^n)^*) \times \mathbb{R}^{a,b} \right\} \tag{2.25}$$

these spaces are dual to each other, and are thefore endowed with a duality pairing:

$$\langle e|f\rangle = \int_Z \langle e_Z(z)|f_Z(z)\rangle dz + e_\partial(b)f_\partial(b) - e_\partial(a)f_\partial(a) \tag{2.26}$$

where the pairing $\langle e_Z(z)|f_Z(z)\rangle$ is the same used in section 2.1. In the characterizing Dirac structures for distributed parameter systems we will use the following concepts:

Definition 2.3 (Differential operator)
Given a nonnegative integer m, an order-m differential operator is a map P from a function space $\mathcal{F}_1$ on $\mathbb{R}^n$ to another function space $\mathcal{F}_2$ that can be written as:

$$P = \sum_{|\alpha| \le m} a_\alpha(x) \frac{\partial^{|\alpha|}}{\partial x_1^{\alpha_1} \partial x_2^{\alpha_2} \cdots \partial x_n^{\alpha_n}} \tag{2.27}$$

Definition 2.4
A differential operator $\mathcal{J}$ on H is *formally skew-adjoint* if it satisfies $\langle \mathcal{J}x|y\rangle = -\langle x|\mathcal{J}y\rangle$ With the functions x and y having 0 boundary conditions at the boundary of the domain.

We have the following result:

Proposition 2.4
The linear subset $\mathcal{D} \subset \mathcal{F} \times \mathcal{E}$ defined by

$$\mathcal{D} = \left\{ (f,e) \in \mathcal{F} \times \mathcal{E} | f_Z = \mathcal{J} e_Z \text{ and } \begin{bmatrix} f_\partial \\ e_\partial \end{bmatrix} (a,b) = e_Z|_{(a,b)} \right\} \tag{2.28}$$

Where $\mathcal{J}$ is a formally skew-adjoint differential operator, is a Dirac structure with respect to the bilinear form (2.2).

This result is a case of proposition 2.2.
Now talk about energy storage and dissipation and power balance

2.3.1 Energy storage

For distributed parameter systems, the Hamiltonian takes the form:

$$H(t) = \int_Z \mathcal{H}(z,\alpha) dz \tag{2.29}$$

where $\mathcal{H}(z,\alpha)$ is an *energy density* function, depending on the position within the spatial domain $z \in [a,b]$ and on the *state* of the system $x : [a,b] \to \mathbb{R}^n$. Flows and efforts within the domain are related to the Hamiltonian as follows:

$$f_Z = \dot{x} \qquad e_Z = \frac{\delta H}{\delta x} \tag{2.30}$$

where $\frac{\delta}{\delta x}$ denotes the *variational derivative* with respect to variable x, which is defined as follows [8]:

Definition 2.5
Consider a functional

$$H[x] = \int_a^b \mathcal{H}\left(z, x, x^{(1)}, \ldots, x^{(n)}\right) dz \tag{2.31}$$

for any smooth real function $x(z), z \in Z$ where the integrand $\mathcal{H}$ is a smooth function of x and its derivatives up to order n. The variational derivative of H with respect to x is the only function that satisfies for every $\varepsilon \in \mathbb{R}$ and smooth real function $\delta x(z), z \in Z$, such that its derivatives satisfy $\delta x^{(i)}(a) = \delta x^{(i)}(b) = 0, i = 0, \ldots, n$:

$$H[x + \varepsilon \delta x] = H[x] + \varepsilon \int_a^b \frac{\delta H}{\delta x} \delta x dz + O(\varepsilon) \tag{2.32}$$

in the case where $\mathcal{H}$ does not depend on the derivatives of x, then the variational derivative is simply $\dfrac{\partial \mathcal{H}}{\partial x}$.

In analogy with the finite-dimensional dynamics formulation in Equation (2.13), we describe the dynamics of distributed parameter port-Hamiltonian systems as:

$$\frac{\partial x}{\partial t} = \mathcal{J} \frac{\delta H}{\delta x} \tag{2.33}$$

2.3.2 Dissipation

To deal with dissipation, we follow the approach in Chapter 6 of [30]. To this end, we rewrite the system dynamics (2.33) in a different form:

$$\frac{\partial x}{\partial t}(t,z)x = \mathcal{J}\mathcal{L}(z)x(t,z) \qquad \alpha(0,z) = x(z) \tag{2.34}$$

where $\mathcal{J}$ is a formally skew-adjoint differential operator and $\mathcal{L}(z)$ is a coercive operator. The efforts are therefore given by $e = \mathcal{L}x(t,z)$.

To include dissipation, we extend our attention to the class of systems described by:

$$\frac{\partial x}{\partial t}(t,z) = (\mathcal{J} - \mathcal{G}_R\mathcal{S}\mathcal{G}_R^*)\mathcal{L}x(t,z), \qquad x(0,z) = x_0(z) \tag{2.35}$$

where $\mathcal{S}$ and $\mathcal{L}$ are bounded coercive operators on $L_2(a,b;\mathbb{R}^m)$ and $X = L_2(a,b,\mathbb{R}^n)$ respectively. The differential operators $\mathcal{J}$ and $\mathcal{G}_R$ are given by:

$$\mathcal{J}x = \sum_{i=0}^{N} P_i\frac{\partial^i x}{\partial z^i} \quad \mathcal{G}_R x = \sum_{i=0}^{N} G_i\frac{\partial^i x}{\partial z^i}, \quad \mathcal{G}_R^* x = \sum_{i=0}^{N}(-1)^i G_i^T\frac{\partial^{(i)} x}{\partial z^i} \tag{2.36}$$

with $\mathcal{G}_R^*$ the formal adjoint of $\mathcal{G}_R$, and G_i, $P_i, i = 1,2,\ldots,N$ constant real matrices of sizes $n \times m$ and $n \times n$ respectively. It is furthermore assumed that these matrices satisfy

$$P_i = (-1)^{i+1}P_i^T \quad i = 0,1,\ldots,N \tag{2.37}$$

and either of the following

$$\begin{bmatrix} P_N & G_N \\ G_N^T & 0 \end{bmatrix} \text{ has full rank,} \qquad \text{if } G_i \neq 0 \text{ for at least one } i \in \{1,2,\ldots,N\} \tag{2.38a}$$

$$P_N \text{ has full rank,} \qquad \text{if } G_i = 0 \text{ for all } i \in \{1,2,\ldots,N\} \tag{2.38b}$$

The interpretation of the new terms introduced in (2.35) is as follows:

- $\mathcal{G}_R$ describes how dissipation comes into the system
- $\mathcal{S}$ describes the amount of dissipation in the system

We rewrite the system with dissipation (2.35) in the following form, by letting $e_r = \mathcal{S}f_r$:

$$\begin{pmatrix} f \\ f_r \end{pmatrix} = \mathcal{J}_e \begin{bmatrix} e \\ e_r \end{bmatrix} = \begin{bmatrix} \mathcal{J} & \mathcal{G}_R \\ -\mathcal{G}_R^* & 0 \end{bmatrix} \begin{bmatrix} e \\ e_r \end{bmatrix} \tag{2.39}$$

The differential operator $\mathcal{J}_e$ is formally skew-adjoint, as $\mathcal{J}$ is formally skew-adjoint itself and $\mathcal{G}_R^*$ is the formal adjoint of $\mathcal{G}_R$.

Example 2.3 (Vibrating string with structural damping)
Let us consider a vibrating string, starting from the lossless case. The string has a 1D domain $Z = [a,b] \subset \mathbb{R}$. The dynamic model is based on the combination of Newton's law and Hooke's law, which yields the wave equation in one dimension:

$$\frac{\partial^2 u(z,t)}{\partial t^2} = \frac{1}{\mu(z)}\frac{\partial}{\partial z}\left(T(z)\frac{\partial u(z,t)}{\partial z}\right) \tag{2.40}$$

where $u(z,t)$ is the transverse displacement of the string, $\mu(z)$ is the mass density of the string, and $T(z)$ is the elastic modulus of the string. We denote by $v(t,z)$ the velocity of the string $v = \frac{\partial u}{\partial t}$. The energy variables of the system $x = [\varepsilon\ p]^\top$ are:

- the strain $\varepsilon(z,t) = \frac{\partial u(z,t)}{\partial z}$
- the elastic momentum $p(z,t) = \mu(z)v(z,t)$

The total energy is given by:

$$H(\varepsilon, p) = U(\varepsilon) + K(p)) \tag{2.41}$$

where $U(\varepsilon)$ is the elastic potential energy:

$$U(\varepsilon) = \int_a^b \frac{1}{2}T(z)(\frac{\partial u(z,t)}{\partial z})^2 dz = \int_a^b \frac{1}{2}T\varepsilon(z,t)^2 \tag{2.42}$$

and $K(p)$ is the kinetic energy:

$$K(p) = \int_a^b \frac{1}{2}\mu(z)v(z,t)^2 dz = \int_a^b \frac{1}{2}\frac{1}{\mu(z)}p^2(z,t) \tag{2.43}$$

We can rewrite the wave equation (2.40) in the form of (2.33)

$$\frac{\partial}{\partial t}\begin{bmatrix}\varepsilon\\ p\end{bmatrix} = \begin{bmatrix}0 & \frac{\partial}{\partial z}\\ \frac{\partial}{\partial z} & 0\end{bmatrix}\begin{bmatrix}\frac{\delta H}{\delta \varepsilon}\\ \frac{\delta H}{\delta p}\end{bmatrix} \tag{2.44}$$

We can introduce structuural damping in the system. The conservation laws for the system now become:

$$\frac{\partial}{\partial t}\begin{bmatrix}\varepsilon\\ p\end{bmatrix} = \frac{\partial}{\partial z}\begin{bmatrix}\frac{p}{\mu}\\ T\varepsilon + k_s\frac{\partial \varepsilon}{\partial z}\left(\frac{p}{\mu}\right)\end{bmatrix} = \begin{bmatrix}0 & \frac{\partial}{\partial z}\\ \frac{\partial}{\partial z} & \left(\frac{\partial}{\partial z}k_s\frac{\partial}{\partial z}\right)\end{bmatrix}\begin{bmatrix}\frac{\delta H}{\delta \varepsilon}\\ \frac{\delta H}{\delta p}\end{bmatrix} \tag{2.45}$$

which can be recast into the form of (2.35) by letting:

$$\mathcal{J} = \begin{bmatrix}0 & \frac{\partial}{\partial z}\\ \frac{\partial}{\partial z} & 0\end{bmatrix}, \quad \mathcal{G}_R = \begin{bmatrix}0\\ \frac{\partial}{\partial z}\end{bmatrix}, \quad \mathcal{S} = k_s > 0, \quad \mathcal{L} = \begin{bmatrix}\frac{1}{\mu} & 0\\ 0 & T\end{bmatrix} \tag{2.46}$$

Let us prove that the differential operator $\mathcal{J}$ in the previous example is indeed formally skew-adjoint. The duality pairing with respect to which we prove skew-adjointedness is:

$$\langle u|v\rangle = \int_a^b uvdz \tag{2.47}$$

we therefore have:

$$\begin{aligned}\langle \mathcal{J}u|v\rangle &= \int_a^b (\mathcal{J}u)vdz\\ &= \int_a^b \left(\frac{\partial u_1}{\partial z}v_2 + \frac{\partial u_2}{\partial z}v_1\right)dz\\ &= \int_a^b \frac{\partial u_1}{\partial z}v_2 dz + \int_a^b \frac{\partial u_2}{\partial z}v_1 dz\end{aligned} \tag{2.48}$$

By applying integratio by parts to both we get:

$$\langle \mathcal{J}u|v\rangle = [u_1v_2 + u_2v_1]_a^b - \int_a^b u_1\frac{\partial v_2}{\partial z}dz - u_2\frac{\partial v_1}{\partial z}dz \tag{2.49}$$

By considering that u and v vanish at the boundary of the domain, we get:

$$\langle \mathcal{J}u|v\rangle = -\langle u|\mathcal{J}v\rangle \tag{2.50}$$

Chapter 3

MFC Valve model

The MFC valves in the ITER GIS are solenoid actuated, normally closed valves. The dynamic model of the valves was divided into two main components: an electromechanical model for the the solenoid, and a flow characteristic that relates mechanical variables of the system to gas flow out of the valve.

3.1 Plunger model

The linear solenoid actuator that operates the valve is modelled through the interaction of two subsystems: a mass-spring-damper, representing the mechanical portion of the actuator, and an RL circuit, for the electric part of the actuator. The interaction between these two subsystems is of electromagnetic nature. As the ferromagnetic plunger within the solenoid moves, the inductance of the RL cuircuit changes, and a magnetic force is exerted on the mass-spring-damper system based on the current flowing through the inductor. Following the PH approach, we may develop models for the two subsystems and then connect them.

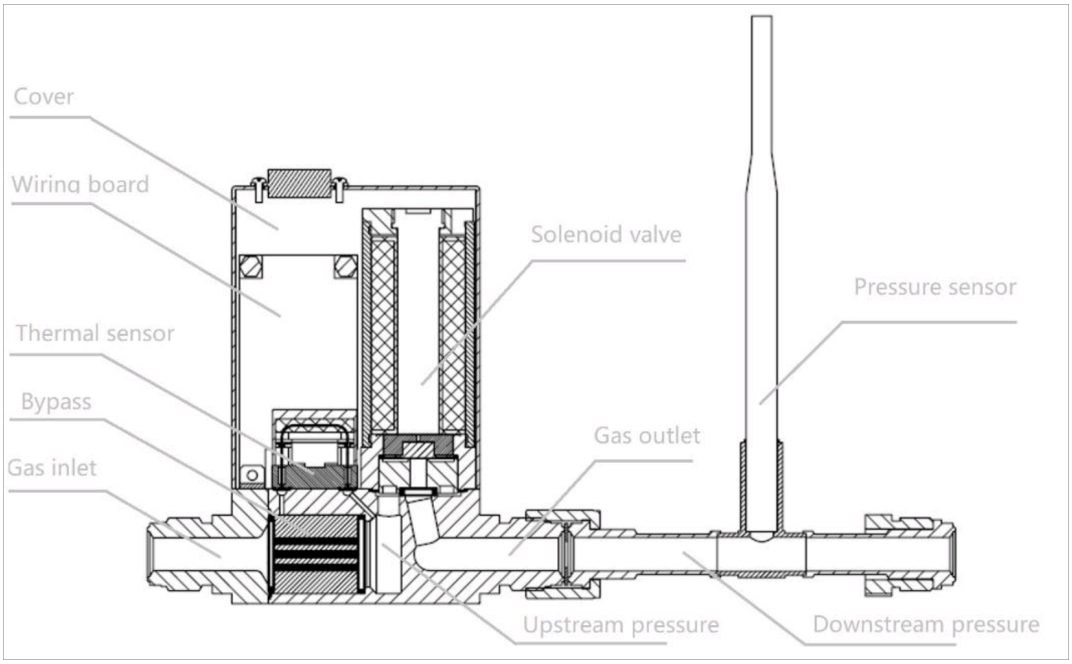

Figure 3.1: Side section of an MFC valve

3.1.1 Mechanical subsystem

The Hamiltonian for the mechanical subsystem is the sum of elastic and kinetic energy:

$$H_m(q,p) = \frac{1}{2}kq^2 + \frac{1}{2m}p^2 \tag{3.1}$$

where q is the position of the plunger and p is its momentum, k is the spring constant and m is the mass of the plunger. The interconnection and damping matrices are:

$$J_m = \begin{bmatrix} 0 & 1 \\ -1 & 0 \end{bmatrix} \quad R_m = \begin{bmatrix} 0 & 0 \\ 0 & b \end{bmatrix} \tag{3.2}$$

where b is the damping coefficient. The dynamic equations for the mechanical subsystem are then

$$\dot{x}_m = [J_m - R_m]\frac{\partial H_m}{\partial x_m} \tag{3.3}$$

where $x_m = \begin{bmatrix} q & p \end{bmatrix}^\top$ is the state of the mechanical subsystem

3.1.2 Electrical subsystem

The Hamiltonian for the electrical subsystem is composed only of the energy stored in the solenoid coil, using as state the flux linkage in the inductor:

$$H_e(\varphi) = \frac{\varphi}{2L} \tag{3.4}$$

Interconnection and damping are trivial:

$$J_e = 0 \quad R_e = R_c \tag{3.5}$$

with R_c the resistance of the RL circuit. The electrical subsystem presents an input voltage, thus the dynamic equation presents as:

$$\dot{x}_e = [J_e - R_e]\frac{dH_e}{dx_e} + gu \tag{3.6}$$

with $g = 1$ and $u = v_{in}$ the input voltage

3.1.3 Coupling the subsystems

Following PH system theory the mechanical and electromechanical subsystems can be interconnected by considering a state space composed of the cartesian product of the state spaces of the subsystems, a Hamiltonian constructed as the sum of the subsystem Hamiltonians and interconnection and damping matrices composed with those of the subsystems. Dependance of the inductance on the plunger position gives the coupling between the mechanical and electrical physical domains.

$$H(q,p,\varphi) = H_m + H_e = \frac{1}{2}kq^2 + \frac{1}{2m}p^2 + \frac{\varphi}{2L(q)} \tag{3.7}$$

$$J = \begin{bmatrix} J_m & 0 \\ 0 & J_e \end{bmatrix} = \begin{bmatrix} 0 & 1 & 0 \\ -1 & 0 & 0 \\ 0 & 0 & 0 \end{bmatrix} \tag{3.8}$$

$$R = \begin{bmatrix} R_m & 0 \\ 0 & R_e \end{bmatrix} = \begin{bmatrix} 0 & 0 & 0 \\ 0 & b & 0 \\ 0 & 0 & 0 \end{bmatrix} \tag{3.9}$$

The dynamic equations of the system can be expressed as

$$\dot{x} = [J - R]\frac{\partial H}{\partial x} + gu \tag{3.10}$$

with $x = \begin{bmatrix} x_m & x_e \end{bmatrix}^\top$, $g = \begin{bmatrix} 0 & 0 & 1 \end{bmatrix}^\top$ and $u = v_{in}$.

Figure 3.2 potrays a bondgraph representing the coupled plunger dynamics. The coupling between the electrical subsystem (on the left) and the mechanical subsystem (on the right) is achieved through an IC field, with the intertial component on the electrical side and the capacitive component on the mechanical side.

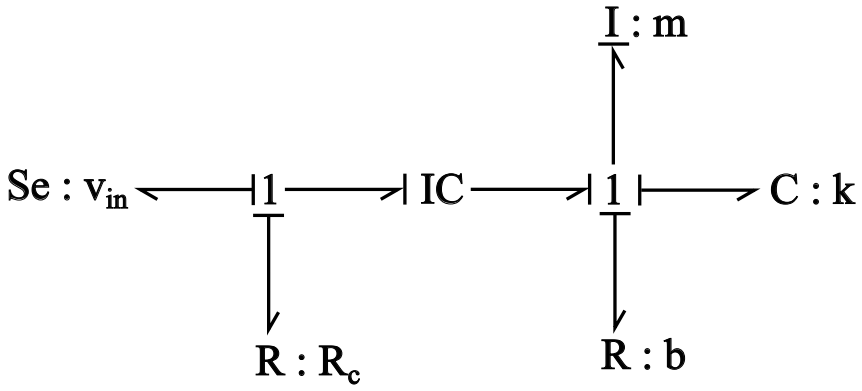

Figure 3.2: Bond graph of the electromechanical dynamics of the solenoid actuated valve

Inductance function

The relation between position of the plunger in the solenoid and inductance is rather complex in its nature, and analytic expressions can be quite involved [27]. For this reason, an approximation of the inductance function based on the experimental work in [25] is used:

$$L(q) = A\left(1 + \frac{q}{c+q}\right) \tag{3.11}$$

By solving $L(q) > 0$ for q, we find that $L(q) < 0$ for $-c < q < -c/2$. Naturally, negative inductance does not make any physical sense. However, in our case the plunger position is constrained to the interval $[0, 1]$, and therefore as long as $c > 0$ inductance is always positive. Figure 3.3 portrays $L(q)$ for the tuned values of its parameters A and c.

3.2 Flow characteristic

The valve is approximated as varying conductance between two pipes. The particle flow, expressed in $Pa \cdot m^3/s$ is given by Bernoulli's equation:

$$Q = \frac{RT}{M}\frac{C_d}{\sqrt{1-\beta^4}}\varepsilon\frac{\pi}{4}d^2\sqrt{2(P_{up} - P_{down})\rho} \tag{3.12}$$

many of these parameters are unknown, and are therefore aggregated into a single one, yielding the following expression:

$$Q = \xi_{gas} C_d \sqrt{\left(P_{up}^2 - P_{down}^2\right)} \tag{3.13}$$

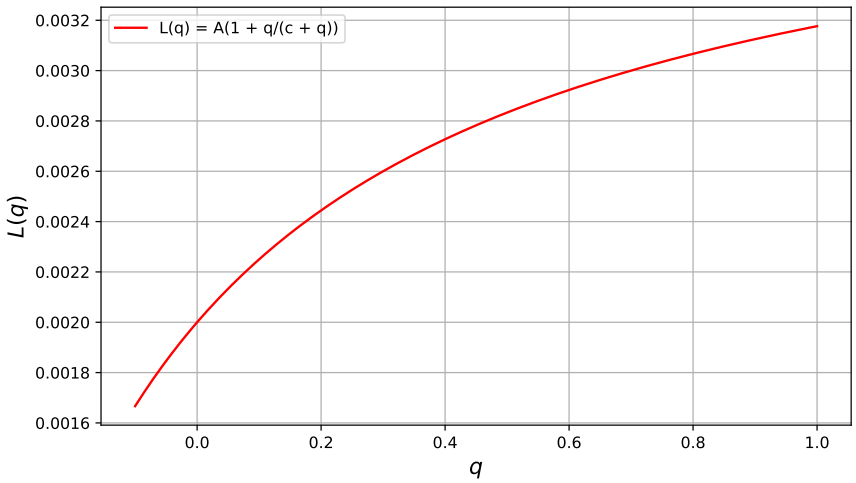

Figure 3.3: Inductance function $L(q)$

3.2.1 Discharge coefficient

The discharge coefficient C_d is a function of the plunger position q. The rationale behind deterimining such function is based on observations made on the experimental data from SWIP. It can be observed by plotting the relation between input voltage and gas flow rate at steady state that it seems to be linear (See fig. 3.4) Based on thes observations,

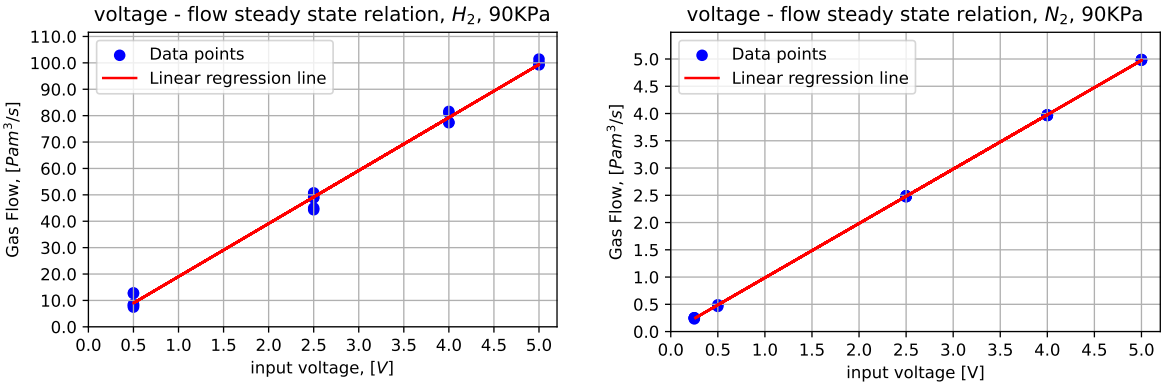

Figure 3.4: Voltage-flow relations at steady state from SWIP data

the discharge coefficient function is crafted to have the same behavior in the simulation model. The chosen function is the product between the plunger position and a number of gaussian functions tuned to obtain this goal:

$$C_d(q) = q(1 + a_1 e^{-b_1(x-d_1)^2})(1 + a_2 e^{-b_2(x-d_2)^2})(1 + a_3 e^{-b_3(x-d_3)^2})(1 + a_4 e^{-b_4(x-d_4)^2}) \quad (3.14)$$

The resulting steady state voltage-flow relation can be seen in figure 3.5

3.2.2 Flow coefficient

The coefficient ξ_{gas} in equation (3.13) was tuned by extracting information on the gas flow rate through the valve at steady state with full aperture from SWIP data, and on pressure

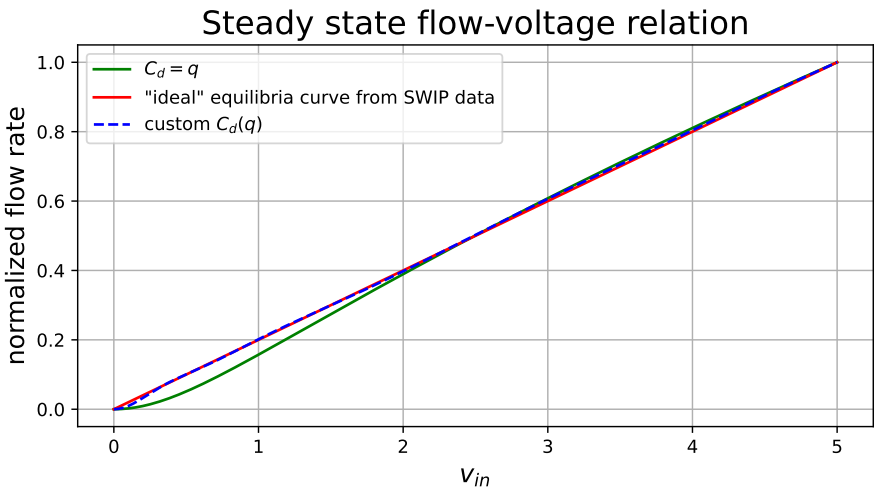

Figure 3.5: simulation model voltage-flow relation at steady state

downstream of the valve from simulations with the pipe model discussed in chapter 4. The pressure upstream of the pipe is assumed to be constant at the value of 90 KPa. The coefficient is thus determined as:

$$\xi_{gas} = \frac{Q_{max}}{\sqrt{P_{up}^2 - P_{down,max}^2}} \tag{3.15}$$

3.3 Sensor model

The MFC valve is equipped with a sensor to measure the flow rate, schematized in figure 3.6. Part of the gas flowing through the valve flows through the sensor. The gas stream through the sensor is warmed up by two heaters (R_{HT1} and R_{HT2} in Fig. 3.6). When the valve is open, the gas transports heat from the first resistor to the second, causing a temperature difference between the two resistors, which, at steady state, is linearly dependent to mass flow rate [31]:

$$\dot{m} = \alpha \Delta T \tag{3.16}$$

Before steady state is reached however, the relation is not as trivial. It can be observed

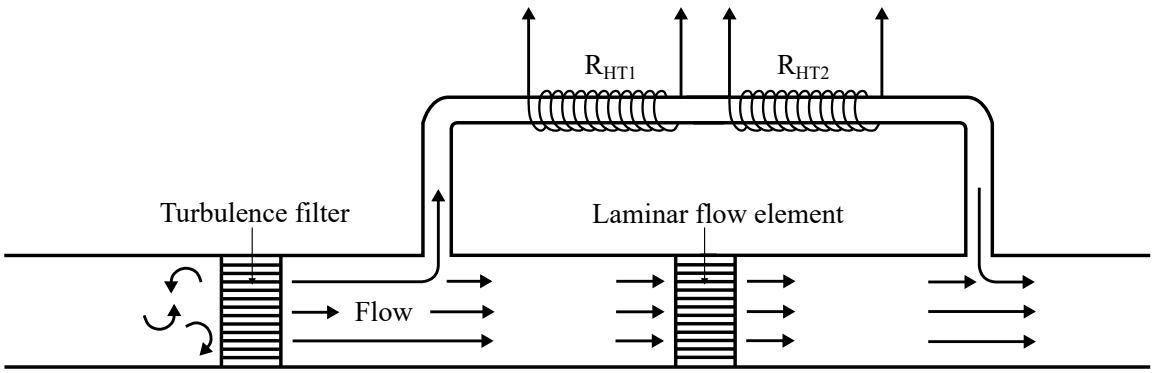

Figure 3.6: Schematic of the MFC valve flow meter

by analyzing experimental data from the SWIP testbench, that the flow sensor seems to respond to changes in the system with some delay compared to the pressure sensor downstream of the MFC valve (see Figure 3.7). This can be explained by taking into account that thermal transport within the moving gas is naturally slower than the flow of gas itself. A very simple way to capture such a behaviour is to model the flow sensor as a low-pass filter, which was the chosen approach. In order for the model of the sensor to be physically sensible, a sought property of the used filter is the lack of overshoot. For this reason, the chosen type of filter is a Bessel low-pass filter, which has the property of providing maximally flat group delay, thus preserving the wave shape of signals in the passband [26].

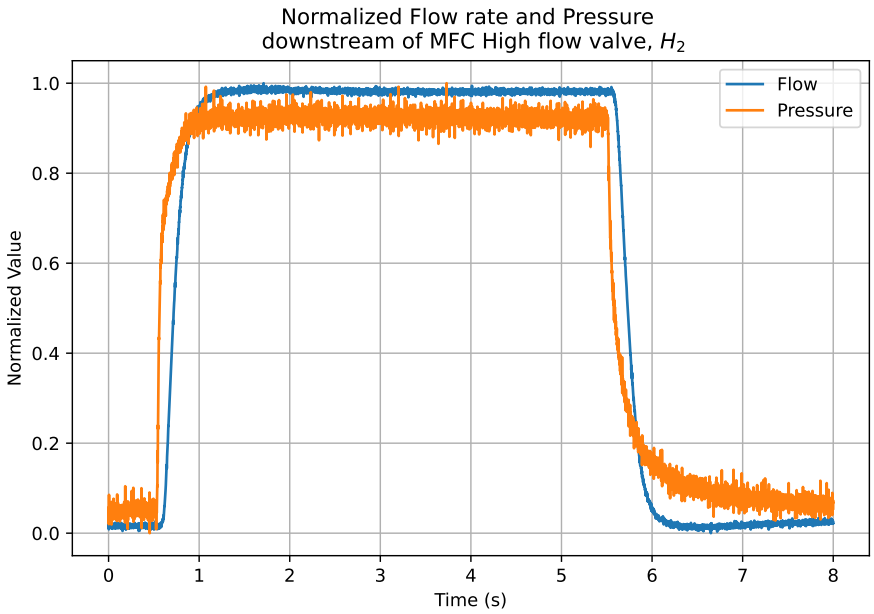

Figure 3.7: Comparison of flow sensor data with pressure downstream of MFC valve

The cutoff frequency for the low-pass filter can be expected to depend on properties of the gas being considered — molar mass, flow rate, temperature, etc. In this case temperature is assumed to always be the same, while gas species and flow rates clearly vary. In particular, the sensor will be slower for heavier gas species and also for slower flowing gas. A different cutoff frequency was tuned for each gas-valve pairing to account for this, with low flow valves getting sensibly lower cutoff frequencies. The tuning was done keeping in mind that the dynamics of the plunger itself remain unchanged across different gasses, and would therefore only depend on the gas species for same type valves (i.e., all high flow valves have the same plunger dynamics and likewise for low flow valves). The different cutoff frequencies can be seen in Table 3.1

The models fo the valve and sensor are implemented in Simulink within the iter Plasma System Simulation Platform. The Simulink model can be seen in Figure 3.8

	cutoff frequency
H_2, high flow	28 rad/s
D_2, high flow	28 rad/s
Ar, low flow	9 rad/s
N_2, low flow	11 rad/s
Ne, high flow	28 rad/s

Table 3.1: flow sensor cutoff frequencies

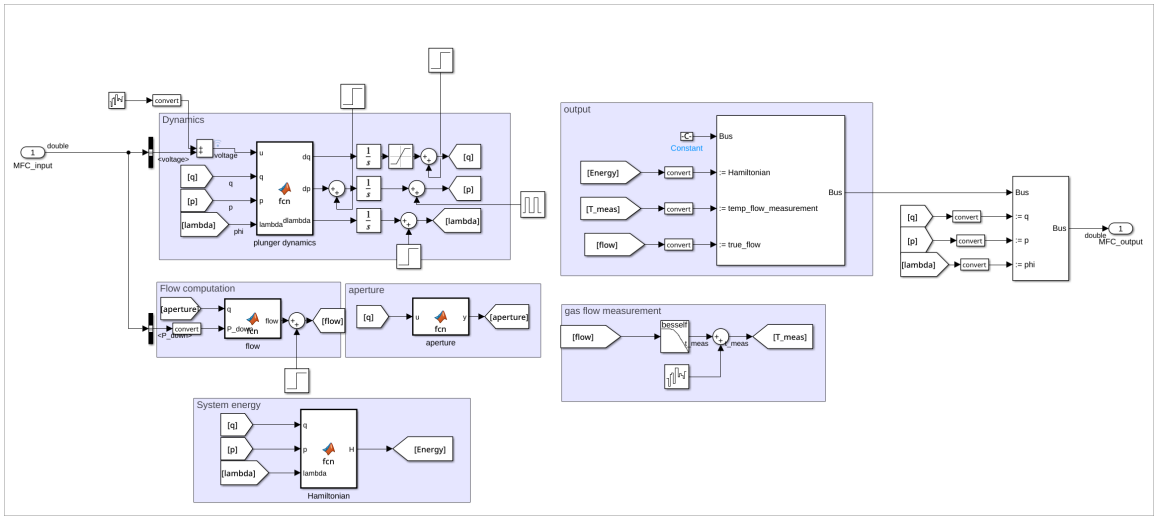

Figure 3.8: Simulink scheme of the MFC valve model.

3.4 Comparison of the simulation model with experimental data

The model was validated against experimental data gathered on a testbench by SWIP The comparison is carried out by feeding the simulation model the same input voltage that was sent to the valve in the experimental test, and the result is considered satisfactory if the flow measured by the simulated sensor sufficiently matches the flow measured by the real sensor.

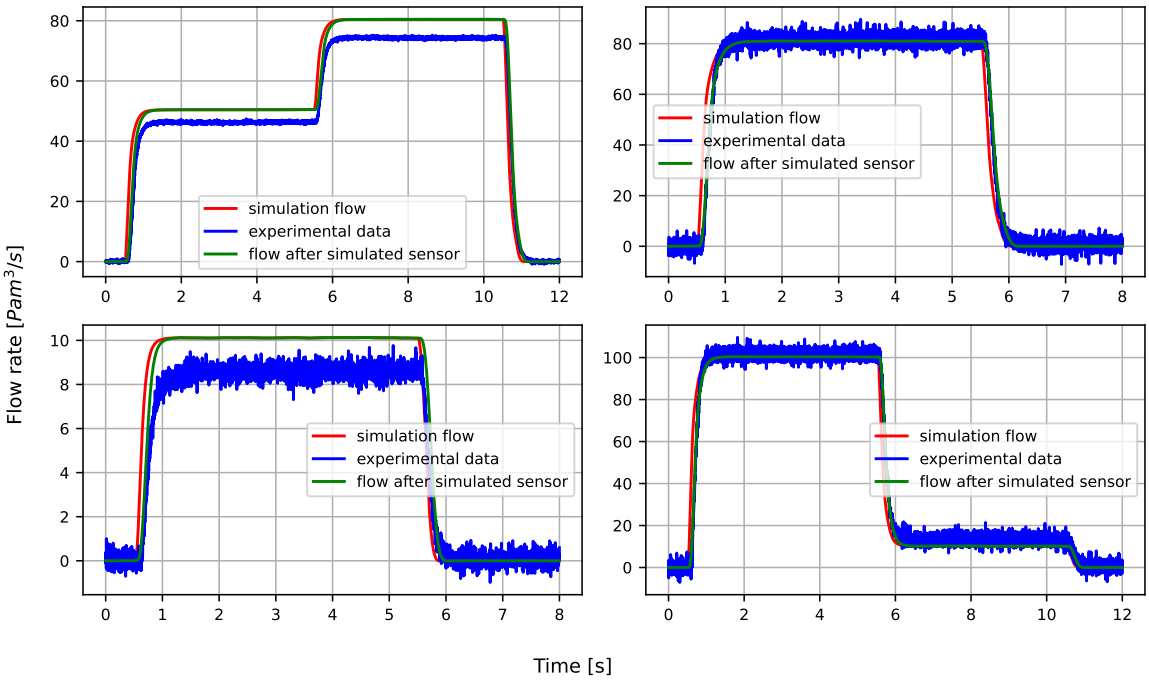

Figure 3.9: Comparison of simulated high flow valve with experimental data, H_2

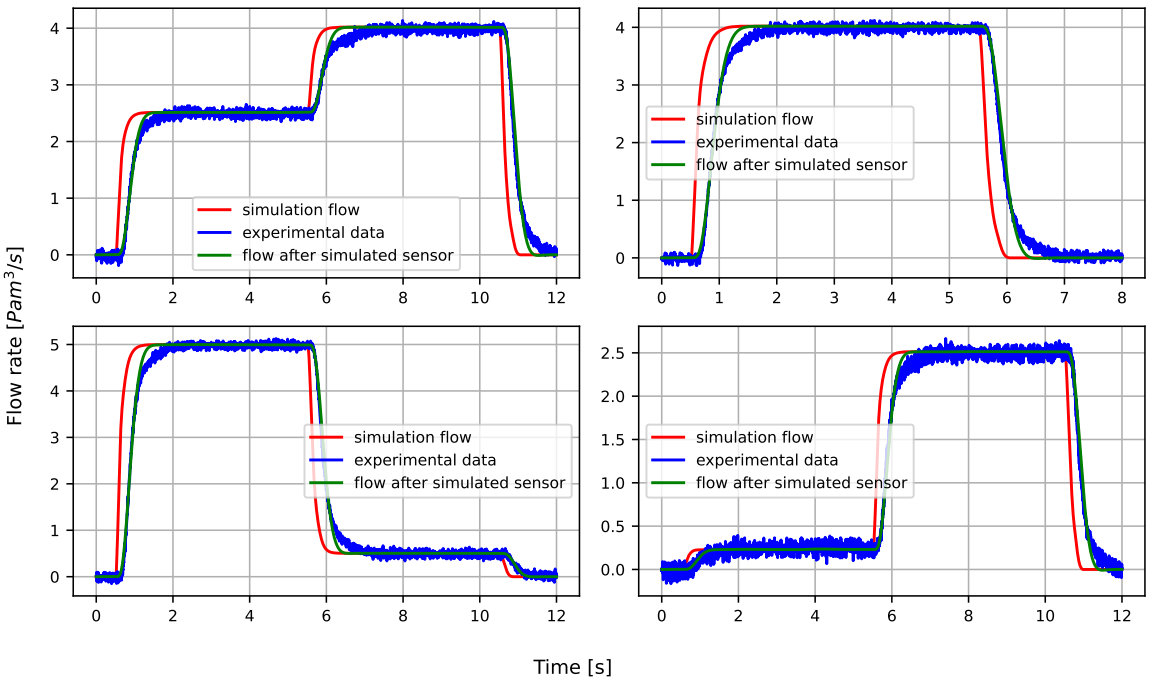

Figure 3.10: Comparison of simulated high flow valve with experimental data, Ar

Chapter 4

Pipe model

A model of the pipes connecting the MFC valves to the vacuum vessel was developed as part of a contract with CEA (Commissariat à l'énergie atomique et aux énergies alternatives). This model was coupled with the MFC valve model presented in chapter 3 for a comprehensive simulation of gas injection. In this chapter, the model is described, along with its coupling with the valve model. A comparison of data produced by simulation of the pipe model with experimental data is carried out, and some alternatives for pipe modelling are presented.

4.1 Model description

The pipe connecting the valve to the vacuum vessel is modelled by a 1D diffusion PDE:

$$\begin{aligned} Q_k(x,t) &= -C_k(x,t)\partial_x P_k(x,t) \\ \partial_t P_k(x,t) &= -\frac{1}{A}\partial_x Q_k(x,t) \end{aligned} \tag{4.1}$$

where the pipe conductance $C_k = C_{k-molecular} + C_{viscous}$ is composed of a molecular and viscous component. The molecular component is computed as

$$C_{k-molecular} = \frac{\pi}{12}\bar{v}_k d^3 \qquad \bar{v}_k = \sqrt{\frac{3RT}{M_k}} \tag{4.2}$$

with d the pipe diameter, $\bar{v}_k$ the molecular velocity, R, T, and M_k respectively the perfect gas constant, the gas temperature and molar mass of gas species k. Viscous conductance is computed as:

$$C_{viscous}(x,t) = \frac{\pi R_0^4}{8\eta(x,t)} \sum_k P_k(x,t) \tag{4.3}$$

where R_0 is the pipe radius and $\eta(x,t)$ is the viscous friction:

$$\eta^{-1}(x,t) = \eta_k^{-1} \frac{M_k P_k(x,t)}{\sum_k M_k P_k(x,t)} \tag{4.4}$$

where η_k is the viscosity of each single gas, computed with Sutherland's formula:

$$\eta_k = \eta_{k-0} \frac{T_{k-0} + C_{k\prime}}{T + C_{k\prime}} \frac{T^{3/2}}{T_k^{3/2}} \tag{4.5}$$

where η_{k-0}, T_{k-0} and $c_{k\prime}$ are respectively the reference viscosity, the reference temperature and Sutherland's constant for the gas species.

4.2 PH formulation of the pipe model

To make the structure of equation (4.1) as a diffusion equation apparent, it can be rewritten as a single equation:

$$\partial_t P_k(x,t) = -\frac{1}{A}\partial_x(-C_k(x,t)\partial_x P_k(x,t)) \tag{4.6}$$

This can be seen as an infinite-dimensional PH system with dissipation (refer to equation in theory part), where:

$$\mathcal{J} = 0, \quad \mathcal{G}_R = \partial_x, \quad \mathcal{S} = \frac{C_k(x,t)}{A} \tag{4.7}$$

It can be easily verified that this satisfies the requirements in section (refer to theory). With the introduction of dissipation flow and effort f_p and $e_p = \mathcal{S} f_p$ the system can be rewritten as:

$$\begin{pmatrix} \partial_t P_k(x,t) \\ f_p \end{pmatrix} = \begin{pmatrix} 0 & \partial_x \\ \partial_x & 0 \end{pmatrix} \begin{pmatrix} P_k(x,t) \\ e_p \end{pmatrix} \tag{4.8}$$

The dissipation flow and effort can be interpreted respectively as particle flow rate diveded by pipe section and as the gradient of pressure in the pipe:

$$e_p = \frac{Q_k(x,t)}{A} \qquad f_p = \partial_x P_k(x,t) \tag{4.9}$$

4.3 Coupling witht valve model

The pipe model interacts with its environment solely through its boundary. In particular, there are four boundary variables: pressure and molecular flow rate at the inlet and outlet of the valve. The model is implemented so that gas flow at the inlet and pressure at the outlet are input variables to the model, while the other two are output variables.

For the inlet, the molecular flow rate is taken from the valve model, sending back the pressure. The (partly symbolic) bond graph of Figure 4.1 depicts this part of the coupling.

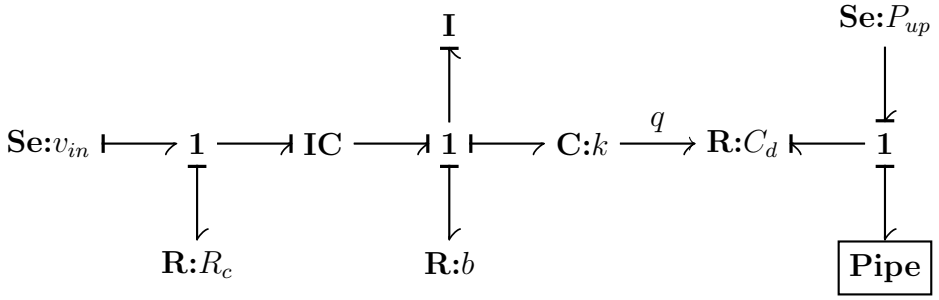

Figure 4.1: bond graph of the coupled pipe and valve

For the outlet, a very simple model of the vacuum vessel is used: The model integrates the difference of the flow rate from the pipe outlet and the pumping speed of the pumps in the vacuum vessel, and based on the volume of the vacuum vessel computes the pressure in the vacuum vessel which is sent to the pipe model as the pressure at the outlet.

4.4 Comparison with experimental data

The pipe model was compared with the data from SWIP to validate it. For this sake, simulations were ran of the coupled valve-pipe system. The same input voltage from the SWIP tests was sent to the valve, and from the pipe model pressure is measured at the inlet of the pipe, in the end portion of the pipe, and inside the vacuum vessel. Data for the pipe model is taken from SWIP datasheets of their simulation setup. Figure 4.2 shows the pressur at the pipe inlet, for both hydrogen through a high flow valve, and argon through a low flow valve. The simulation results are not too fare off from the experimental results. However, looking at Figure 4.3, which depicts pressure towards the end of the pipe, we see that for the high flow case, the model predicts far more pressure than is present, while in the low flow case it predicts much less. Finally, Figure 4.4 shows the pressure inside the vacuum vessel. In this case, the datasheet values for the pumping speed of the vacuum vessel were not used. Instead, the effective pumping speed was estimated directly from experimental data. With this approach, a good matching of the simulation model with the experimental data was obtained.

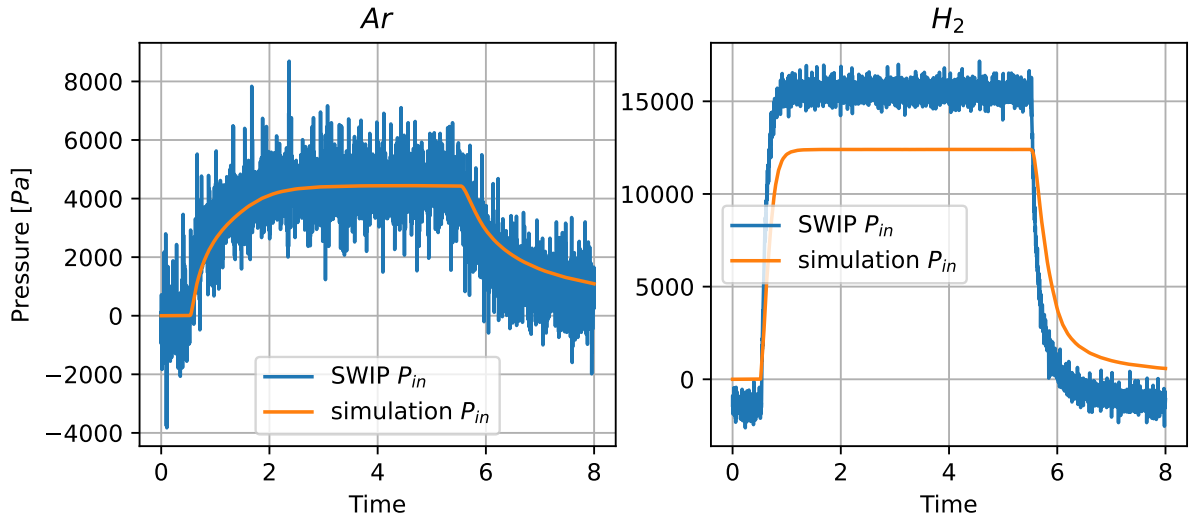

Figure 4.2: Pressure at the pipe inlet

insert plots of comparison, talk about datasheet values for pumping speed and why we change them willy-nilly, talk about negative pressure readings and mismatch of data with simulation model, difference in timing of transients. Specify model is part of CEA contract. Talk about options to modify/change model, why only tuning will not help.

In some of the plots of the experimental data, negative values of pressure are present. This is obviously not physically possible, however it can be attributed to sensor noise and/or offset that is within the specifications of the sensors.

It is to be noted that while the model does not accurately capture the behaviour of the system, what is most important is the prediction of the flow at the gas outlet. Unfortunately, no flow meter was installed at the pipe outlet in the SWIP tests, therefore no flow measurement at the outlet is available for comparison with the pipe model.

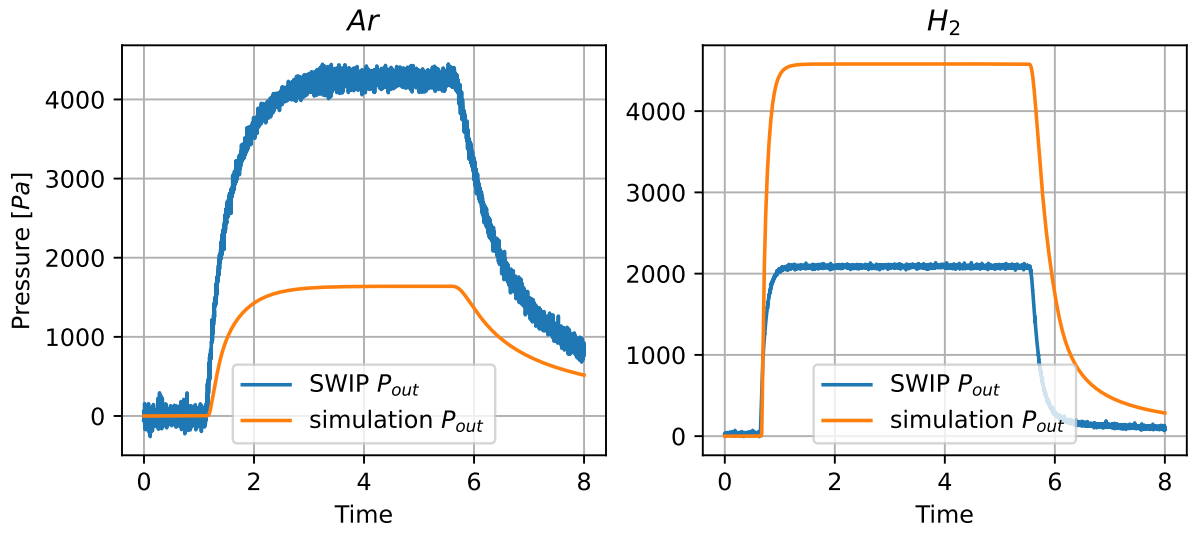

Figure 4.3: Pressure at the end of the pipe

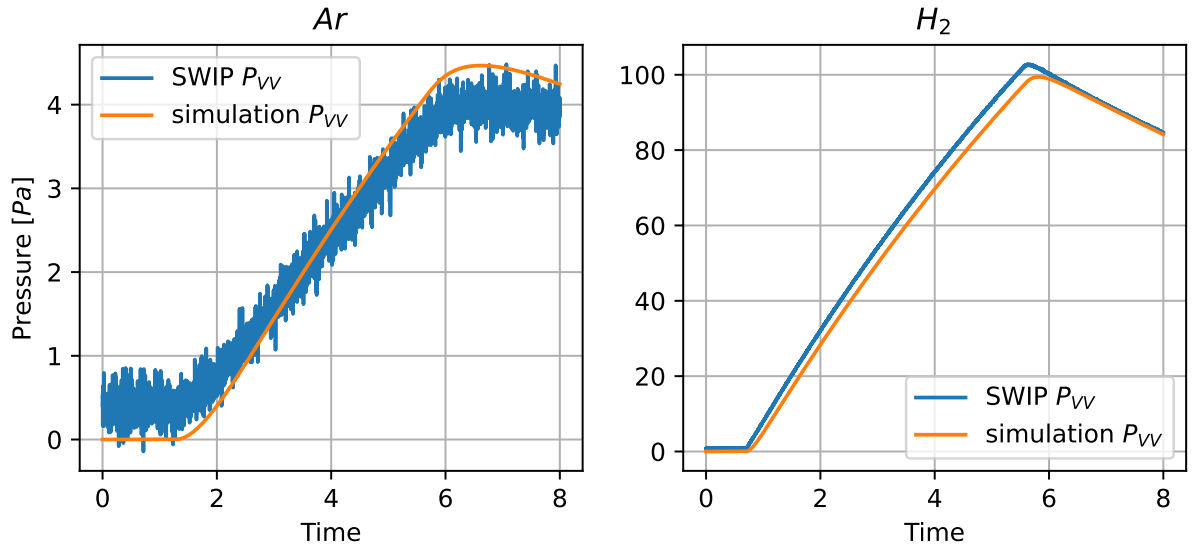

Figure 4.4: Pressure in the vacuum vessel

4.5 Alternative pipe models

Two main potential alternatives were identified for the pipe model: the first is to augment the existing model with a trasport term, thus obtaining an Advection-Diffusion equation. The second is to change approach entirely, and to instead use a model based on the isothermal Euler equations.

4.5.1 Advection-Diffusion model

The Advection-Diffusion model is obtained by adding a transport term to the diffusion equation (4.6):

$$\partial_t P_k(x,t) = -\frac{1}{A}\partial_x(-C_k(x,t)\partial_x P_k(x,t)) + U\partial_x(Q_k(x,t)) \tag{4.10}$$

The main idea behind this approach is that diffusion describes gas motion well at slow speeds and small pressure, while transport becomes more relevant at higher speeds. This might help make the model more accurate overall.

Advection-Diffusion (or Convection-Diffusion) models can be cast in the PH formulation as shown in [30]. The difference with what presented for the Diffusion model in section 4.2 is that the differential operator $\mathcal{J}$ becomes

$$\mathcal{J} = U\partial_x \tag{4.11}$$

4.5.2 Euler model

An alternative, popular in modelling gas networks [7], is to use the isothermal Euler equations. We consider for a first overview the Euler equations in the case of no friction and with a horizontal pipe. The model is formulated as:

$$\begin{aligned} \partial_t \rho &= -\partial_x(\rho v) \\ \partial_t(\rho v) &= -\partial_x(\rho v^2 + P) \end{aligned} \tag{4.12}$$

where:

- ρ is the gas density
- v is the stream velocity
- P is the gas Pressure
- x is the spatial variable aligned with the length of the pipe
- t is time

Pressure and density can be related as follows:

$$P = c^2\rho \tag{4.13}$$

with c the speed of sound in the gas, thus obtaining:

$$\begin{aligned} \partial_t \rho &= -\partial_x(\rho v) \\ \partial_t(\rho v) &= -\partial_x(\rho v^2 + c^2\rho) \end{aligned} \tag{4.14}$$

We wish to use as state variables ρ and v, therefore we must reformulate the equations. By differentiating using the chain rule, we obtain:

$$\partial_t(\rho v) = \rho\partial_t v + v\partial_t\rho \tag{4.15}$$

$$\partial_x(\rho v) = \rho\partial_x v + v\partial_x\rho \tag{4.16}$$

By applying these relations to (4.14) we obtain:

$$\begin{aligned} \partial_t \rho &= -\partial_x(\rho v) \\ \partial_t v &= -\frac{c^2}{\rho}\partial_x \rho - v\partial_x v \end{aligned} \tag{4.17}$$

We now have a pair of conservation laws. We must identify a suitable Hamiltonian function for the system. We consider a function of the following form:

$$H = \int_L \mathcal{H}(\rho, v)dx \tag{4.18}$$

where the enrgy density function $\mathcal{H}$ is of the form

$$\mathcal{H} = \frac{1}{2}\rho v^2 + \rho U(\rho) \tag{4.19}$$

where the first term represents kinetic energy and the second a general potential energy function. We wish to write the system in the form:

$$\partial_t \begin{pmatrix} \rho \\ v \end{pmatrix} = \begin{pmatrix} 0 & -\partial_x \\ -\partial_x & 0 \end{pmatrix} \begin{pmatrix} \frac{\delta H}{\delta \rho} \\ \frac{\delta H}{\delta v} \end{pmatrix} \tag{4.20}$$

By comparing our desired form of the dynamics with what obtained above we get, by looking at the time derivative of velocity:

$$-\partial_x \left(\frac{v^2}{2} + U(\rho) + \rho U'(\rho) \right) = -\frac{c^2}{\rho}\partial_x \rho - v\partial_x v \tag{4.21}$$

here $U'(\rho)$ is the derivative of $U(\rho)$ with respect to ρ. By manipulating the left side we get

$$v\partial_x v + (2U'(\rho) + \rho U''(\rho))\partial_x \rho = -\frac{c^2}{\rho}\partial_x \rho - v\partial_x v \tag{4.22}$$

and thus obtain the ODE

$$2U''(\rho) + \rho U'(\rho) = \frac{c^2}{\rho} \tag{4.23}$$

which has as solution

$$U(\rho) = c^2 \log(\rho) + \frac{c_1}{\rho} + c_2 \tag{4.24}$$

with c_1, c_2 integrating constants.

Chapter 5

MFC Valve control

The control scheme for the valve is composed of two main components: an observer to reconstruct the state of the valve, and a controller that uses this information to steer the system to a desired setpoint or trajectory. Both the observer and the control law have been implemented in discrete-time in accordance with the requirements for the ITER Control System. It is to be noted that the controller was developed with the assumption that the state of the valve be known, thus creating the need for an observer to infer such information.

5.1 Observer

In order to build the observer the state is extended by adding the flow rate measured by the flow sensor as it has dynamic behaviour wrt the state of the plunger, and is renamed $\xi = [x\ Q_m]^\top$ with Q_m the measured flow rate. The chosen structure for the observer is that of a Luenberger observer with added integral action:

$$\hat{\xi}_{k+1} = f_d(\hat{\xi}_k, u_k) + K_P(\hat{y} - y) + K_I \sum_{t=0}^{k} (\hat{y} - y) \tag{5.1}$$

where f_d is the discretized valve dynamics, obtained through the Runge-Kutta method for the plunger dynamics, and through the least-squares method using MATLAB's `c2d()` function to discretize the Bessel filter transfer function for the sensor dynamics.

In Figure 5.1 the behaviour of the observer with white noise on the flow measurement is displayed for a high flow valve, while in Figure 5.2 the behaviour of the observer when a force step is applied to the plunger at $t = 3s$ can be seen.

As can be seen in the disturbed case (Fig. 5.2) plunger momentum and flux linkage estimates do not converge to the real values. This is not a problem as the controller only needs to ensure that the plunger position reaches its reference to achieve the desired flow rate.

5.2 Reference Generation

The designed controller focuses on controlling the plunger subsystem. As such, it tracks references for the state of the plunger as described in subsection 3.1. In order for the controller to be of use for the control system, it is therefore to be taken into account that references for the control system are given in terms of flow rate. It is therefore necessary to

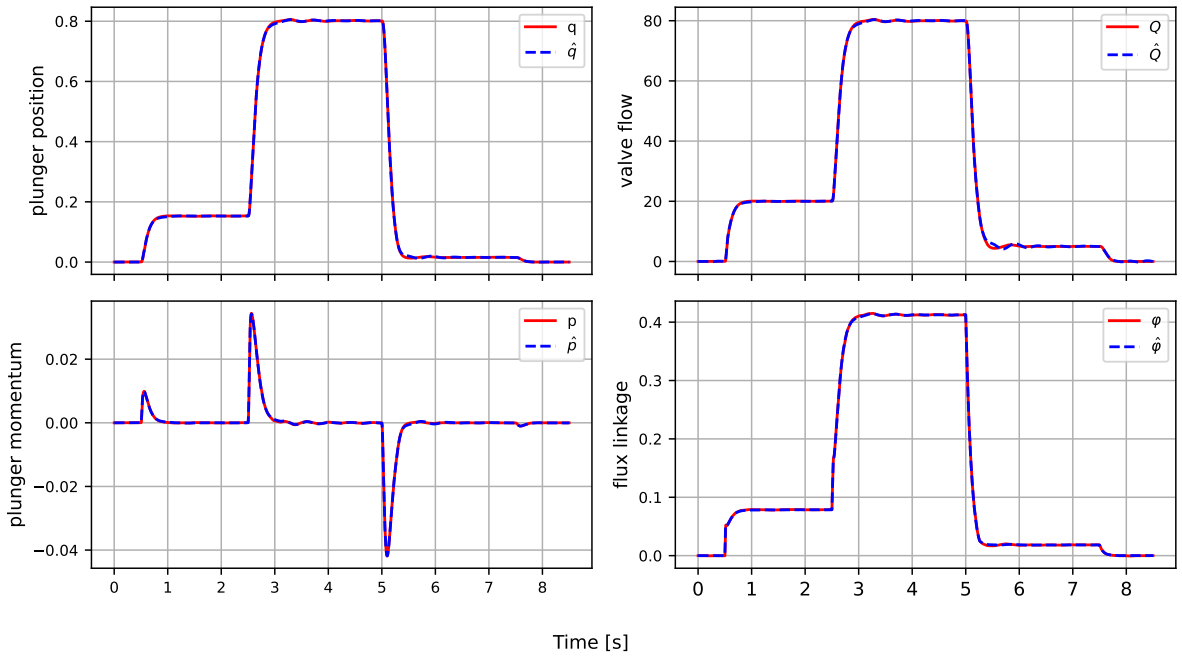

Figure 5.1: observer estimates of valve state

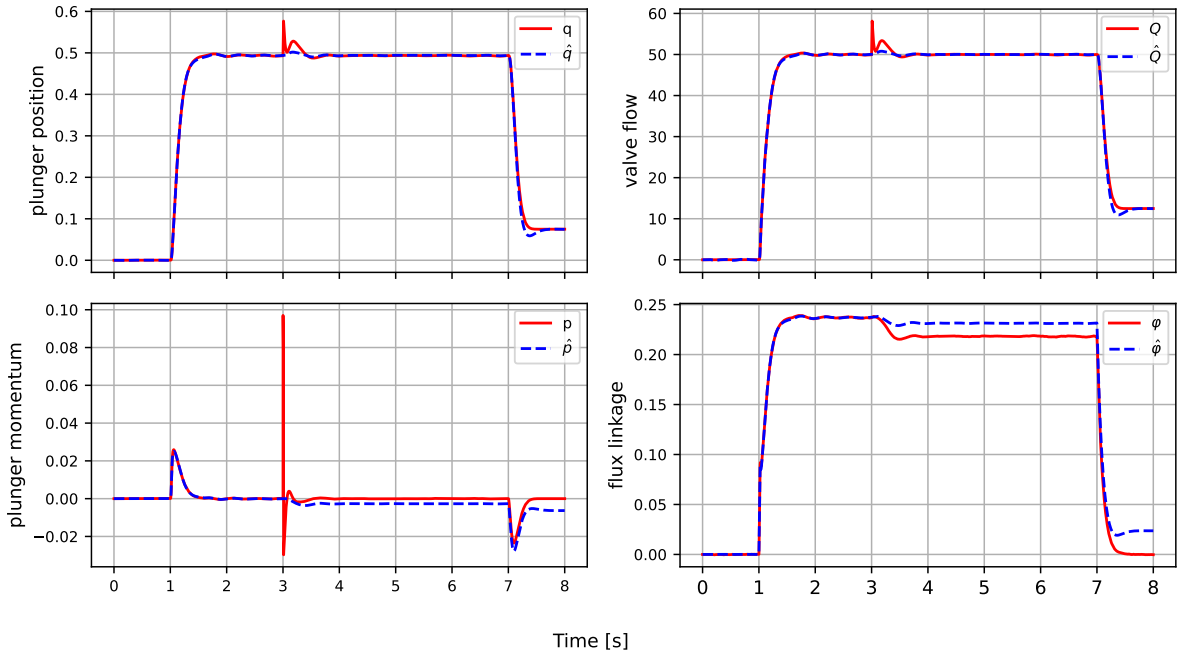

Figure 5.2: observer estimates of valve state

translate flow references into references for the state of the plunger. This can be achieved by inverting the flow characteristic of the valve, obtaining the desired plunger position. The open loop valve dynamics can then be solved to find the required steady state flux linkage, and for static references the desired momentum will be 0.

5.3 IDA-PBC controller

Control is developed for the electromechanical subsystem described in subsection 3.1. The chosen control scheme is IDA-PBC [17], following the Algebraic approach to solving the matching equation. A quadratic desired energy function is selected:

$$H_d(q,p,\varphi) = \frac{\gamma_1}{2}(q-q^\star)^2 + \frac{p^2}{2m} + \frac{\gamma_2}{2}(\varphi-\varphi^\star)^2 \tag{5.2}$$

A general form for the desired interconnection (J_d) and damping (R_d) matrices is considered at first, along with a trivial option for the left annihilator of g:

$$\begin{aligned} J_d(x) &= \begin{bmatrix} 0 & J_{1,2} & J_{1,3} \\ -J_{1,2} & 0 & J_{2,3} \\ -J_{1,3} & -J_{2,3} & 0 \end{bmatrix} \quad R_d(x) = \begin{bmatrix} r_1 & 0 & 0 \\ 0 & r_2 & 0 \\ 0 & 0 & r_3 \end{bmatrix} \\ g^\perp &= \begin{bmatrix} 1 & 0 & 0 \\ 0 & 1 & 0 \end{bmatrix} \end{aligned} \tag{5.3}$$

The matching condition thus yields a set of two equations:

$$\begin{cases} \dfrac{p}{m} = -r_1\gamma_1(q-q^\star) + J_{12}\dfrac{p}{m} + J_{13}\gamma_2(\varphi-\varphi^\star) \\ -kq + \dfrac{\varphi^2}{2L^2(q)}\dfrac{dL}{dq} - b\dfrac{p}{m} == -\gamma_1(q-q^\star) - r_2\dfrac{p}{m} + J_{23}\gamma_2(\varphi-\varphi^\star) \end{cases} \tag{5.4}$$

Solving the matching equation yields the following:

$$\begin{aligned} &J_{1,2} = 1,\ J_{1,3} = 0,\ r_1 = 0,\ r_2 = b,\ \gamma_1 = k \\ &J_{2,3} = \frac{1}{\gamma_2(\varphi-\varphi^\star)}\left(\frac{\varphi^2}{2L^2(q)}\frac{dL}{dq} - kq^*\right) \end{aligned} \tag{5.5}$$

leaving as freely assignable the parameters γ_2 and r_3, respectively related to closed loop magnetic energy storage and electric damping. The control law can be computed as

$$\begin{aligned} (g^\top g)^{-1}g^\top \left[(J_d - R_d)\frac{\partial H_d}{\partial x} - (J-R)\frac{\partial H}{\partial x}\right] = \\ = -J_{2,3}\frac{p}{m} - r_3\gamma_2(\varphi-\varphi^\star) + \frac{R_c\varphi}{L(q)} \end{aligned} \tag{5.6}$$

the control effort is singular for the desired equilibrium, in particular for $\varphi = \varphi^\star$. It is to be noted that in steady state, (one very relevant occasion in which $\varphi = \varphi^\star$), we would also have $p = 0$. Solving the closed loop dynamics for steady state conditions, with the added caveat of considering $J_{23} = 0$ when its denominator vanishes (thus giving a well defined value to the controller in that situation), yields the desired equilibrium. In practice, a threshold for $(\varphi - \varphi^\star)$ under which $J_{2,3}$ is set to 0 is chosen.

The resilience of the system to steady state disturbances was also tested. A step force is applied to the valve plunger at $t = 3s$, and as can be seen in Figs. 5.5 and 5.6 the system converges back to the desired equilibrium.

The observer and controller are both implemented in Simulink within the iter Plasma System Simulation Platform. The Simulink models can be seen in Figure 5.8 and 5.7

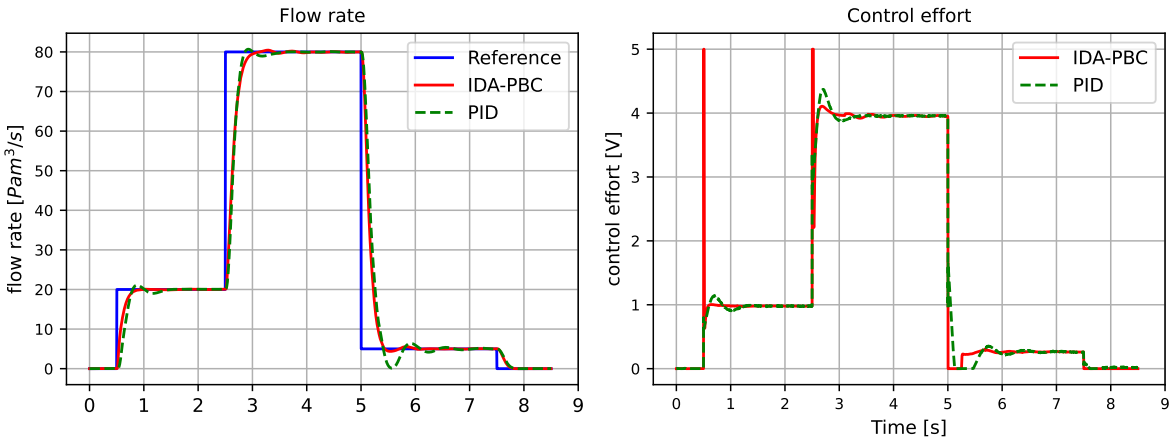

Figure 5.3: result of IDA-PBC control on high flow valve with H_2

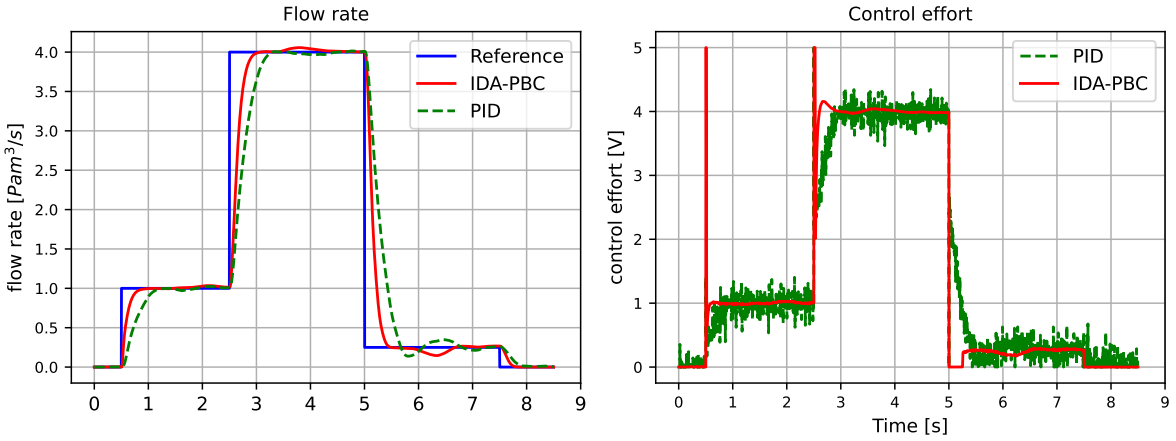

Figure 5.4: result of IDA-PBC control on high flow valve with Ar

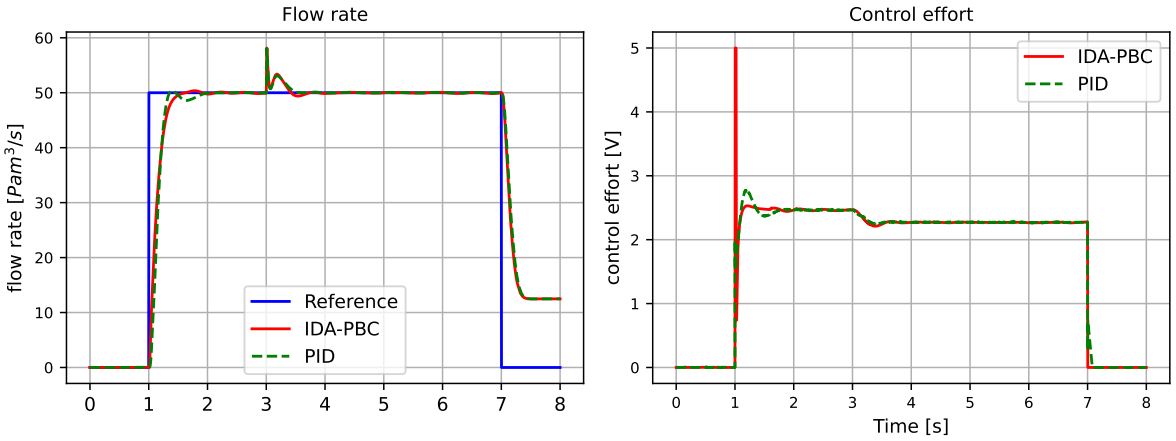

Figure 5.5: high flow valve with step force disturbance at $t = 3s$, H_2

5.4 Alternative control functions

While the Algebraic approach is what was ultimately used, it is still interesting to explore the outcomes of the Parametrized and Non-Parametrized approaches to crafting a control

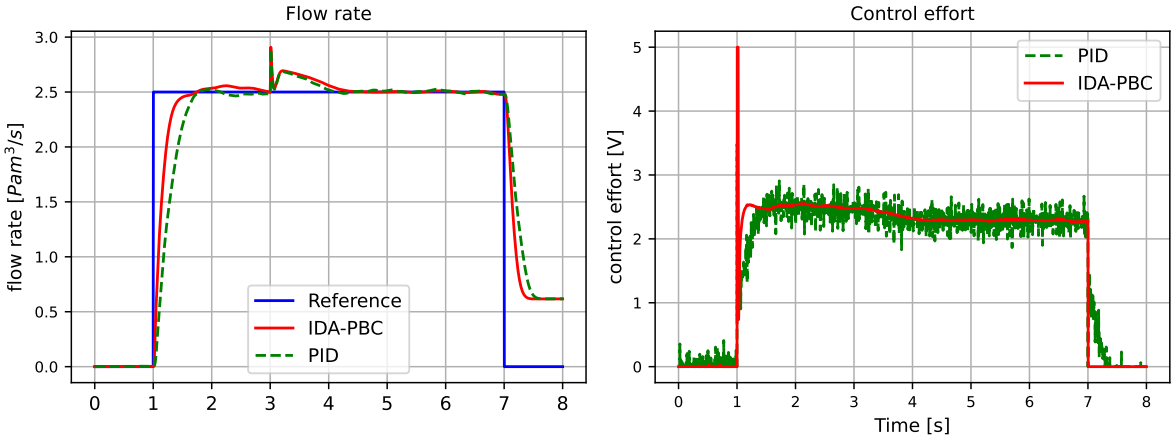

Figure 5.6: low flow valve with step force disturbance at $t = 3s$, Ar

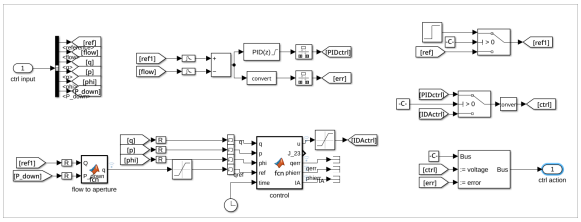

Figure 5.7: Controller Simulink model

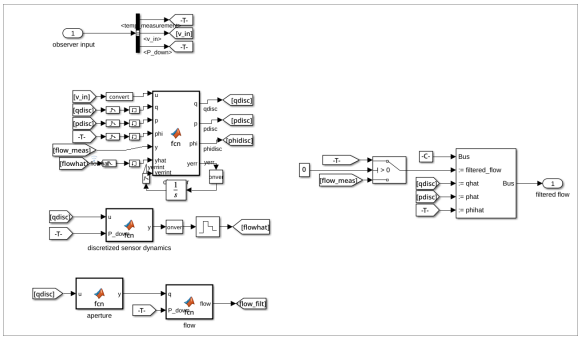

Figure 5.8: Observer Simulink model

function. The results are presented as an exploratory exercise as they were out of the scope of this work having achieved a working control scheme, and were therefore not pursued to completion.

5.4.1 Parametrized IDA

Based on physical intuiton, we set the following form for the desired closed loop Hamiltonian:

$$H_d(q, p, \varphi) = \frac{1}{2m}p^2 + \chi(q, \varphi) \tag{5.7}$$

we consider the same generic J_d, R_d and $g^\perp$ as in (5.3). Imposing the matching condition we obtain the following:

$$\begin{cases} \dfrac{p}{m} = -r_1 \dfrac{\partial \chi}{\partial q}(q, \varphi) + J_{12}\dfrac{p}{m} + J_{13}\dfrac{\partial \chi}{\partial \varphi}(q, \varphi) \\ -kq + \dfrac{\varphi^2}{2L^2(q)}\dfrac{dL}{dq} - b\dfrac{p}{m} = -J_{12}\dfrac{\partial \chi}{\partial q}(q, \varphi) - r_2\dfrac{p}{m} + J_{23}\dfrac{\partial \chi}{\partial \varphi}(q, \varphi) \end{cases} \tag{5.8}$$

from which we get:

$$J_{1,2} = 1,\ J_{1,3} = 0,\ r_1 = 0,\ r_2 = b \tag{5.9}$$

$$-kq + \frac{\varphi^2}{2L^2(q)}\frac{dL}{dq} = \frac{\partial \chi}{\partial q}(q, \varphi) + J_{23}\frac{\partial \chi}{\partial \varphi}(q, \varphi) \tag{5.10}$$

Taking $J_{23} \neq 0$, equation (5.10) turns out to be a non-homogeneous transport PDE. The reader is referred to appendix A for more details on the method used to solve PDEs of similar structure. We start by rewriting the PDE in a more amenable form:

$$\frac{\partial \chi}{\partial q}(q,\varphi) - J_{23}\frac{\partial \chi}{\partial \varphi}(q,\varphi) = +kq - \frac{\varphi^2}{2L^2(q)}\frac{dL}{dq} \tag{5.11}$$

We employ the change of coordinates:

$$(q,\varphi) \to (\xi,\varphi) = (-J_{23}q - \varphi, \varphi) \tag{5.12}$$

and look for a solution in the these coordinates

$$v(\xi,\varphi) = \chi(q,\varphi) \tag{5.13}$$

The solution to the PDE is then:

$$\begin{aligned} v(\xi,\varphi) &= -\frac{1}{J_{23}}\int_0^{\varphi} \omega(\xi,\lambda)d\lambda + g(J_{23}q - \varphi) \\ \omega(\xi,\varphi) &= -k\frac{\xi+\varphi}{J_{23}} - \frac{\varphi}{2L^2\left(\frac{\xi+\varphi}{J_{23}}\right)}\frac{dL}{d\left(\frac{\xi+\varphi}{J_{23}}\right)}\left(\frac{\xi+\varphi}{J_{23}}\right) \end{aligned} \tag{5.14}$$

with $g(J_{23}q - \varphi)$ a function to be assigned. Among the family of solutions, one must choose one such that the conditions in (2.17) are satisfied.

5.4.2 Non-Parametrized IDA

With the Non-Parametrized approach, we fully fix the desired closed loop structure of the system. In this case, we may observe that the main obstacle in control is the lack of coupling between the electromagnetic and mechanical physical domains. For this reason, we consider as desired interconnection and damping matrices:

$$J_d = \begin{bmatrix} 0 & 1 & 0 \\ -1 & 0 & -\alpha \\ 0 & \alpha & 0 \end{bmatrix} \qquad R_d = R \tag{5.15}$$

The desired Hamiltonian remains to be fully determined from the matching condition. By imposing it, we obtain (much similarly to (2.20), however with nonlinear terms that make the solution much more cumbersome):

$$\frac{\partial H_a}{\partial q} - \alpha\frac{\partial H_a}{\partial \varphi} = \alpha\frac{\varphi}{L(q)} \tag{5.16}$$

as in the Parametrized case we obtain a 2D diffusion PDE with a source term. By changing once again to characteristic coordinated, we compute a solution in the form

$$v(\xi,\varphi) = H_a(q,\varphi), \qquad \xi = -\alpha q + \varphi \tag{5.17}$$

the solution once again comes from integration:

$$\begin{aligned} v(\xi,\varphi) &= \frac{1}{\alpha}\int_0^{\varphi} \omega(\xi,\lambda)d\lambda + g(-\alpha q + \varphi) \\ \omega(\xi,\varphi) &= -\frac{\alpha\lambda}{A}\left(\frac{-\alpha q + \lambda + c}{2(-\alpha q + \lambda) + c}\right) \end{aligned} \tag{5.18}$$

The solution of the integral is:

$$\int_0^{\varphi} \omega(\xi, \lambda) d\lambda = \frac{1}{A} \left[\frac{c(2q\alpha - c) ln(2\lambda - 2q\alpha + c) + 2\lambda^2 + 2c\lambda}{8A} \right]_{\lambda=0}^{\varphi} \tag{5.19}$$

The function $g(-\alpha q + \varphi)$ is to be chosen such that the conditions in (2.17) are satisfied.

As can be noted by the last two sections, finding closed form solutions for the control function is a non-trivial task. The Algebraic approach was chosen as it was the most straightforward to implement and provided satisfactory results. The other two approaches can greatly benefit from the use of numerical solvers rather than finding closed form solutions for the energy function through the matching equation. It can also be noted that the control law from the Algebraic approach has the benefit of being a generally simpler function, at least in the considered case.

Chapter 6

Conclusion

This thesis presents a dynamic model of solenoid-actuated MFC valves intended for use in the ITER GIS system, as well as a model for the piping connecting the valves to the vacuum vessel. The models were tested against experimental data to validate them. The MFC valve model achieved satisfactory results, while the pipe model was found to lack some accuracy. Other options for pipe modelling were proposed. An observer and controller for the MFC valve were developed, tested in simulation, and their performance and robustness to disturbances were successfully validated. The proposed control strategy demonstrates superior effectiveness compared to a PID controller, particularly in scenarios where flow sensor limitations are most significant, such as in the case of low-flow valves, by minimizing overshoot.

The work was carried out exploiting the port-Hamiltonian framework, which was briefly presented. This framework aided in crafting a multiphysics model of the valves, as well as a naturally stable controller.

The work presented in this thesis is part of a larger project at ITER, which aims to develop a density control scheme for the plasma. The models and simluations presented aid in assessing the functionality of the GIS as part of the density control scheme, as well as identifying potential challenges and technological constraints in operations of the tokamak.

The continuation of this project would involve further developement of the gas pipe model, with particular attention to the effects of gas mixtures within the pipes. From the control point of view, a control scheme exploiting the use of multiple gasses in the same pipe, in particular the seeding of impurities through fuelling gasses to expedite their arrival in the vacuum vessel.

Appendix A

Solution of transport PDEs

In this appendix, the problem of solving the matching equation coming from IDA-PBC is tackled, in a way that aims at finding closed-form solutions to the PDEs rising from this type of problem. What rises from the matching equation can be seen as a transport PDE with a source term (see sections 5.4.1 and 5.4.2). In the following, a method for solving 2D equations, based on the method of characteristics described in [16, 9].

Given a PDE of the form

$$au_x + bu_y = f(x, y) \tag{A.1}$$

we seek for a solution $u(x, y)$ satisfying it. The method of characteristics is based on a change of variables, putting the problem in *characteristic coordinates*. Characteristics are curves along which the homogeneous solution to the PDE are constant. The change of coordinates is:

$$(x, y) \to (\xi, y) = (bx - ay, y) \tag{A.2}$$

and we seek for a solution to the equation in characteristic coordinates

$$v(\xi, y) = u(x, y) \tag{A.3}$$

By applying the chain rule, we can write the derivatives of v in terms of the derivatives of u:

$$\begin{aligned} \partial_x u = \partial_x v = \partial_\xi v \partial_x \xi + \partial_y v \partial_x y = b\partial_\xi v \\ \partial_y u = \partial_y v = \partial_\xi v \partial_y \xi + \partial_y v \partial_y y = -a\partial_\xi v + \partial_y v \end{aligned} \tag{A.4}$$

We may thus recast the problem in characteristic coordinates, obtaining the following PDE:

$$au_x + bu_y = abv_\xi + bv_y - abv_\xi = f(x, y) \tag{A.5}$$

which can be simplified to:

$$v_y = \frac{f(\frac{\xi + ay}{b}, y)}{b} \tag{A.6}$$

where we have recast $f(x, y)$ in terms of the characteristic coordinates. The solution is then obtained simply by integration:

$$v(\xi, y) = \frac{1}{b} \int_0^y f(\frac{\xi + as}{b}, s)ds + g(\xi) \tag{A.7}$$

with $g(\xi)$ an arbitrary function of ξ only. The solution in the original coordinates is then obtained by reverting the change of coordinates:

$$(\xi, y) \to (x, y) = \left(\frac{\xi + ay}{b}, y\right) \tag{A.8}$$

Bibliography

[1] D. Archer and S. Rahmstorf. *The Climate Crisis: An Introductory Guide to Climate Change*. Cambridge University Press, 2009.

[2] John Stewart Bell. Hamiltonian mechanics. 1987.

[3] Alexandre Bovet. *Suprathermal ion transport in turbulent magnetized plasmas*. PhD thesis, 02 2015.

[4] Stas Burek. When will fossil fuels finally run out and what is the technical potential for renewable energy resources? *International Journal of COMADEM*, 13(4), 2010.

[5] M. B. Chadwick and B. Cameron Reed. Introduction to special issue on the early history of nuclear fusion. *Fusion Science and Technology*, 80(sup1):iii–xxi, 2024.

[6] P.C. de Vries and et al. Strategy to systematically design and deploy the ITER plasma control system: A system engineering and model-based design approach. *Fusion Engineering and Design*, 204:114464, 2024.

[7] Pia Domschke, Benjamin Hiller, Jens Lang, Volker Mehrmann, Riccardo Morandin, and Caren Tischendorf. Gas network modeling: An overview. 2021.

[8] Vincent Duindam, Alessandro Macchelli, Stefano Stramigioli, and Herman Bruyninckx. *Modeling and Control of Complex Physical Systems: The port-hamiltonian approach*. Springer, Germany, 2009.

[9] R. Haberman. *Applied Partial Differential Equations: With Fourier Series and Boundary Value Problems*. Pearson Prentice Hall, 2004.

[10] D.C. Karnopp, D.L. Margolis, and R.C. Rosenberg. *System Dynamics: Modeling, Simulation, and Control of Mechatronic Systems*. Wiley, 2012.

[11] W. Li, B. Li, S. Maruyama, T. Jiang, Y. Yang, Z.W. Xia, Y.X. Zhang, and J. Lu. A description of the iter's gas injection systems and current r&d activities. *Fusion Engineering and Design*, 87(5):813–821, 2012. Tenth International Symposium on Fusion Nuclear Technology (ISFNT-10).

[12] Philippe Magaud, G. Marbach, and Ian J. Cook. Nuclear fusion reactors. 2004.

[13] B. Maschke and A. van der Schaft. Port-controlled Hamiltonian systems: modelling origins and system theoretic properties. In *Nonlinear Control Systems Design 1992*, pages 359–365. Elsevier, 1993.

[14] Jürgen Meyer-ter Vehn, Stefano Atzeni, and Rafael Ramis. Inertial confinement fusion. *Europhysics news*, 29(6):202–205, 1998.

[15] D. Oh, M. Choe, G. Baek, D. Kim, B. K. Jung, K. J. Chung, I. Kourakis, and C. Sung. Development of a new magnetic mirror device at the korea advanced institute of science and technology. *Journal of Plasma Physics*, 90(2):975900202, 2024.

[16] P.J. Olver. *Introduction to Partial Differential Equations*. Undergraduate Texts in Mathematics. Springer International Publishing, 2013.

[17] R. Ortega and E. Garcia-Canseco. Interconnection and damping assignment passivity-based control: towards a constructive procedure - part i. In *2004 43rd IEEE Conference on Decision and Control (CDC) (IEEE Cat. No.04CH37601)*, volume 4, pages 3412–3417 Vol.4, 2004.

[18] Romeo Ortega, Arjan van der Schaft, Bernhard Maschke, and Gerardo Escobar. Interconnection and damping assignment passivity-based control of port-controlled hamiltonian systems. *Automatica*, 38(4):585–596, 2002.

[19] Henry M. Paynter. *Analysis and Design of Engineering Systems: Class Notes for M.I.T. Course 2.751*. M.I.T. Press, Cambridge, Massachusetts, 1960.

[20] Raymond Pierrehumbert. There is no plan b for dealing with the climate crisis. *Bulletin of the Atomic Scientists*, 75(5):215–221, 2019.

[21] Richard Pitts, Richard Buttery, and Simon Pinches. Fusion: the way ahead. *Physics World*, 19(3):20, mar 2006.

[22] T. Ravensbergen and et al. Strategy towards model-based design and testing of the ITER Plasma Control System. *Fusion Engineering and Design*, 188:113440, 2023.

[23] Mutaz Ryalat, Dina Shona Laila, Hisham ElMoaqet, and Natheer Almtireen. Dynamic ida-pbc control for weakly-coupled electromechanical systems. *Automatica*, 115:108880, 2020.

[24] Mutaz Ryalat, Dina Shona Laila, and Mohamed M. Torbati. Integral ida-pbc and pid-like control for port-controlled hamiltonian systems. In *2015 American Control Conference (ACC)*, pages 5365–5370, 2015.

[25] D. Szpica and Michał Kusznier. Model evaluation of the influence of the plunger stroke on functional parameters of the low-pressure pulse gas solenoid injector. *Sensors*, 21:234, 01 2021.

[26] Marc T. Thompson. Chapter 14 - analog low-pass filters. In Marc T. Thompson, editor, *Intuitive Analog Circuit Design (Second Edition)*, pages 531–583. Newnes, Boston, second edition, 2014.

[27] Hossein Vahid Alizadeh and Benoit Boulet. Analytical calculation of the magnetic vector potential of an axisymmetric solenoid in the presence of iron parts. *IEEE Transactions on Magnetics*, 52(3):1–4, 2016.

[28] A. van der Schaft. Port-Hamiltonian Modeling for Control. *Annual Review of Control, Robotics, and Autonomous Systems*, 3(1):393–416, 2020.

[29] A. van der Schaft and D. Jeltsema. *Port-Hamiltonian Systems Theory: An Introductory Overview*. Foundations and Trends® in Systems and Control Series. Now Publishers, 2014.

[30] J.A. Villegas. *A Port-Hamiltonian Approach to Distributed Parameter Systems*. Phd thesis - research ut, graduation ut, University of Twente, Netherlands, May 2007.

[31] M. Viswanathan, A. Kandaswamy, S. K. Sreekala, and K. V. Sajna. Development, modeling and certain investigations on thermal mass flow meters. *Flow Measurement and Instrumentation*, 12(5):353–360, January 2002.